VAASAN AMMATTIKORKEAKOULU
UNIVERSITY OF APPLIED SCIENCES

Timo Uimonen

MATHEMATICAL MODELLING OF METAL-AIR BATTERY

Technology and Communication
2018

VAASAN AMMATTIKORKEAKOULU
Energia- ja ympäristötekniikka

TIIVISTELMÄ

Tekijä	Timo Uimonen
Opinnäytetyön nimi	Mathematical Modelling of Metal-Air Battery
Vuosi	2018
Kieli	englanti
Sivumäärä	58
Ohjaaja	Asseri Laitinen

Tämän opinnäytetyön tavoitteena oli kehittää matemaattinen malli ja simulaatio magnesium-ilma-akulle. Niiden avulla voidaan analysoida akkukennon suorituskykyä kokeellisista tuloksista valituilla suunnitteluparametreillä. Opinnäytetyö tehtiin VEBIC:lle, joka on Vaasan yliopiston isännöimä tutkimus- ja innovaatioalusta.

Mallinnettavan akkukennon komponentit valittiin julkaistujen tutkimustulosten perusteella. Tämän pohjalta aloitettiin kehittämään magnesium-ilma-akun matemaattista mallia, joka muodostui massatasapainon ja sähkökemiallisen kinetiikan yhtälöiden numeerisista ratkaisuista. Akkukennon laskennallinen simulaatio kehitettiin Python-ohjelmointikielellä.

Opinnäytetyön tuloksena syntyi magnesium-ilma-akun malli, jonka antamat tulokset olivat sopusoinnussa kokeellisten arvojen kanssa. Sen avulla voitiin ennustaa akkukennon suorituskykyä valituissa olosuhteissa. Jatkossa mallia voidaan hyödyntää magnesium-ilma-akun suorituskyvyn optimoinnissa.

Avainsanat	Mallinnus, simulaatio, metalli-ilma-akku ja numeeriset menetelmät

VAASAN AMMATTIKORKEAKOULU
UNIVERSITY OF APPLIED SCIENCES
Energia- ja ympäristötekniikka

ABSTRACT

Author	Timo Uimonen
Title	Mathematical Modelling of Metal-Air Battery
Year	2018
Language	English
Pages	58
Name of Supervisor	Asseri Laitinen

The aim of this thesis was to develop a mathematical model and simulation of magnesium-air battery. Together, they can provide insight into the performance of the battery with respect to the design parameters obtained from experimental data. The thesis was carried out at VEBIC, a research and innovation platform hosted by the University of Vaasa.

In the first step, literature was reviewed which helped to identify active materials of the cell. In the second step, the mathematical model of magnesium-air battery was developed. This entailed solving the mass balance and electrochemical kinetic equations by using numerical methods. Finally, a computational simulation of the cell was developed in Python programming language.

The thesis resulted in a development of magnesium-air battery model. The model output corroborated with experimental data. It predicted cell performance under chosen operating conditions. Going forward, the model could be utilized to optimize magnesium-air battery performance.

Keywords Modelling, numerical methods, metal-air battery and simulation

ACKNOWLEDGMENT

I would like to start with thanking my supervisor, Asseri Laitinen, for his assistance during the thesis. I would also like to thank the former director of VEBIC, Dr. Krish Sankaran, for introducing me to this topic and giving me the opportunity to work on this thesis at VEBIC. I owe my deepest gratitude to Abbos Shodiev for his guidance throughout the thesis. This thesis would not have been possible without his assistance. I would also like to offer my special thanks to Pankaj Kela and Dr. Joel Songok for proofreading the thesis and offering me valuable feedback. Lastly, I would like to thank my family for all their support.

CONTENTS

LIST OF FIGURES AND TABLES

LIST OF SYMBOLS AND ABRIVATIONS

Abbreviations

ORR	Oxygen reduction reaction
OVITO	Open visualization tool
HEV	Hydrogen evolution reaction
PVA	Polyvinyl alcohol
PEO	Polyethylene oxide
LiSICON	A protective glass-ceramic layer for Li metal
SEM	Scanning electron microscope
SHE	Standard hydrogen electrode
IDE	Integrated development environment

Symbols

J	Flux of species
D	Diffusion coefficient
C	Concentration of species
$c_{j,x}$	Concentration of species x at a point j
$c_{i,x}$	Concentration of species x at a point i that is connected to point j
z	Charge of electroactive species
F	Faraday's constant
R	Gas constant
T	Temperature

t	Duration of the discharge
m	Mass of active material
a	Height of the anode/Area of the reactive surface of the anode
x_a	Width of the anode
V	Hydrodynamic velocity
n	Number of exchanged electrons in the reaction
F	Faraday's constant
$E°$	The Standard potential
E	Potential under nonstandard conditions
E_{eq}	Equilibrium potential
G	Gibbs free energy
k^o	Rate of reaction
S	Sink term
A	Frequency factor
E_a	Activation energy of species
i_f	Forward current
i_b	Backward current
i_o	Exchange current density
i_j	Current density
i_{load}	Applied load current
C_{ah}	Capacity of the cell

$\partial C/\partial x \partial y$	Concentration gradient
$\partial \Phi/\partial x \partial y$	Electric gradient
β	Charge transfer coefficient
ρ	Density of species
η	Overpotential

1 INTRODUCTION

Energy storage is becoming increasingly vital and popular topic in today's society. We depend on stored energy in our daily lives. Phones, laptops and cars, all require stored energy to function. Climate change has driven technological development towards renewable solutions which have led to a new frontier of challenges /1–3/. Many renewable energy sources, such as solar and wind, are characterised by intermittency. At present, the solar or wind energy cannot be solely relied upon as a primary energy source without utilization of energy conversion and storage. /1, 3/. Furthermore, the forecasted increase in adaptation of low emission hybrid and electric vehicles will also lead to an increased demand for stored energy /4, 5/. However, the current battery technology does not meet the requirements of rapidly advancing technology. The maximum energy density of current lithium-ion batteries has been deemed insufficient for high energy applications such as electric vehicles. /6–8/. Therefore, a great research effort has been devoted to the development of the next generation high energy density metal-air batteries /7, 9/.

The purpose of this thesis was to develop a two-dimensional mathematical model and a computational simulation for a primary magnesium-air battery. Together, they can provide a tool to analyse the performance of the battery with respect to design parameters obtained from experimental data. The mathematical model and the simulation were developed for Vaasa Energy Business Innovation Centre (VEBIC) which is a research and innovation platform hosted by the University of Vaasa.

The mathematical model focuses on the electrode-electrolyte interactions. The scope of the thesis was limited to the main reactions at the electrodes and precipitation of magnesium hydroxide ($Mg(OH)_2$) in the electrolyte. The effects of corrosion and other parasitic reactions were not considered.

The thesis is composed of two main segments: a theoretical framework and a simulation. The theoretical framework centres around the creation of the mathematical model. It begins with the introduction of metal-air batteries, the cell chemistry and the structure. It will then move on to an overview of magnesium-air batteries and the configuration of the cell that is being modelled. The remaining part focuses on the governing equations which are the heart of the mathematical model. The governing equations describe the essential

cell behaviour in mathematical terms. It also contains a description of assumptions on which the model is built.

The simulation segment covers a description of the methodology which includes numerical methods and different tools used to build the simulation. It also contains a list of parameters used in the computational simulation. The results & discussion section presents the results of the simulation and compares the results to previously published experiments.

2 METAL-AIR BATTERIES

Metal-air batteries have received much attention from researchers as a promising candidate for a new generation of energy storage. This is due to their much higher theoretical energy density and lower material cost than traditional batteries. The basic principle behind metal-air battery cells is similar to the electrochemical cell. The cell generally comprises negatively charged electrode, also known as an anode; positively charged electrode known as a cathode; and an electrolyte, which functions as a two-way transport medium for ions and as a separator between the electrodes to avoid short circuit. What makes metal-air batteries to stand out from traditional batteries, is their open cell structure. Unlike traditional batteries, metal-air batteries use oxygen obtained from an external source as reactive material at the cathode, hence the name metal-air battery. /6, 10–12/. This makes metal-air batteries very similar to fuel cells which also use oxygen gas as reactive material at the cathode /6–7/. However, unlike hydrogen fuel cells, metal-air batteries offer many advantages, such as simple structure, solid fuel storage and low cost /13/.

The usage of oxygen, obtained from the surroundings, as active material is what allows metal-air batteries to have many times the energy density of traditional batteries /10/**.** Figure 1 shows a Ragone plot that benchmarks different energy storage technologies /14/. The plot shows power density as a function of energy density. In terms of energy density, the metal-air batteries come second only to that of fuel cells while also having higher power density. It is noteworthy that metal-air batteries are still in research stage. Therefore, data provided in Figure 1 may change during the development of metal-air batteries.

Metal-air batteries have potential applications as energy storage for renewable energy systems, range extenders for electric vehicles and other. They are often classified according to the material used in anode. The most common anode materials for metal-air batteries include lithium, magnesium and zinc. Table 1 compares the properties of the common anode material. Metal-air batteries can function either as secondary batteries, meaning they are rechargeable, or as primary batteries implying that they are not rechargeable. Despite not being rechargeable, many primary metal-air batteries have been considered mechanically rechargeable where the anode material can be physically replaced. The metal-air battery supplies power by converting chemical energy into electrical energy through oxidation-reduction reaction. /6, 10–12, 15/

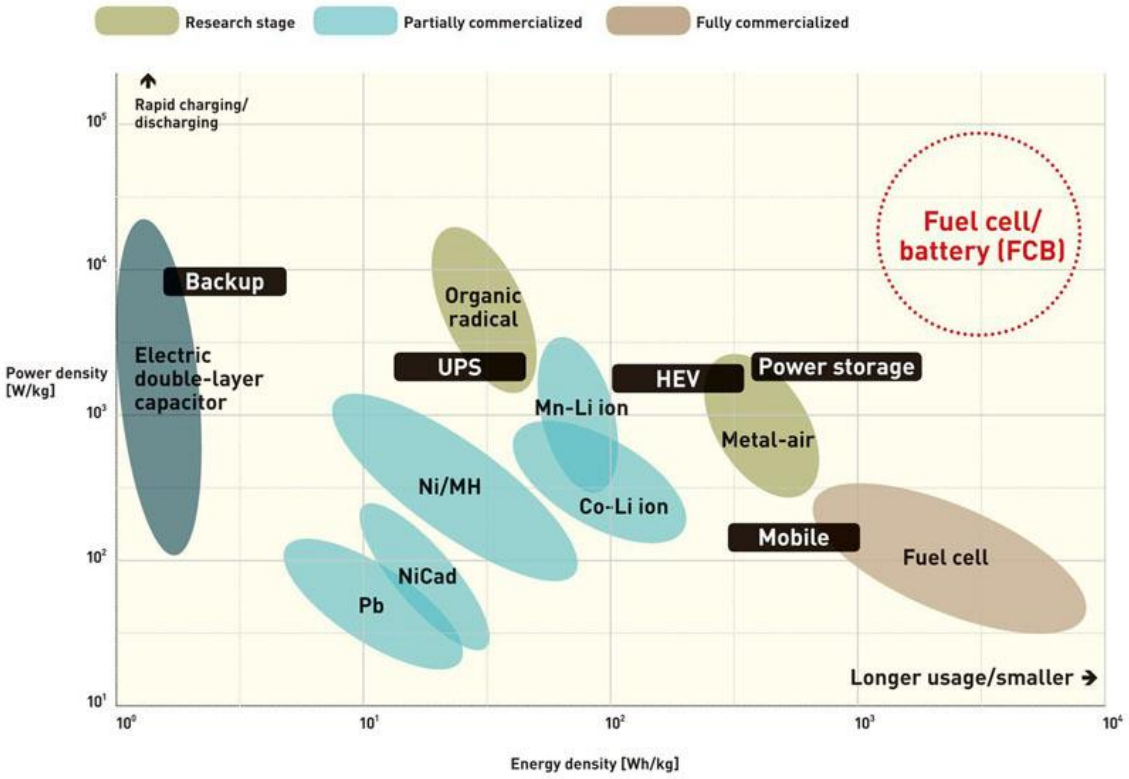

Figure 1. Ragone plot comparing power and energy densities of different energy storage systems /14/.

Table 1. Comparison of specifications of different metal-air batteries /15/.

Batteries	Theoretical Voltage (V)	Theoretical specific capacity (Ah Kg^{-1})	Theoretical energy density (kWh kg^{-1})	Practical operating voltage (V)
Li—air	3.4	1170	13.0	2.4
Zn—air	1.6	658	1.3	1.0—1.2
Mg—air	3.1	920	6.8	1.2—1.4
Na—air	2.3	687	1.6	2.3
Al—air	2.7	1030	8.1	1.2—1.6

2.1 Functioning Principle

The key reaction in the working of a metal-air battery is oxidation-reduction reaction, which is also called a redox-reaction. In the redox-reaction, the electrodes will either become oxidized or reduced through transfer of electrons. The redox-reaction is often described in general redox-reaction equation (equation 1), where the *O* symbolizes oxidized form, *n* is the number of electrons e^- transferred and *R* symbolizes the reduction

form. /16/. This reaction converts chemical potential energy into electrical work. During the discharge, the battery functions as a galvanic cell, in which the chemical reaction occurs spontaneously at both electrodes when they are connected via an external conductor (Figure 2). If the cell is rechargeable, it would function as an electrolytic cell while being connected to an external current source. Redox reactions are often described in half-reactions at electrodes. /17, 18/

$$O + ne^- \rightleftharpoons R \quad (1)$$

In a galvanic cell, the first half-reaction is called oxidation, which occurs at the anode. During the oxidation, the metal in the anode releases electrons, thus oxidized. During this process, the metal atoms become positively charged ions due to loss of electrons. The release and movement of electrons will create an electric current that can be used in different applications. The electrons will be transferred to the cathode via a metal conductor, also known as a current collector, due to potential difference between the two electrodes. The metal ions at the anode will undergo a dissolvent reaction in which they will dissolve into electrolyte as a result. /16–17/

The second half-reaction is called a reduction reaction. The reduction reaction occurs in the cathode, a feature distinguishing metal-air battery from the other types of batteries. In a typical battery, the reduction happens between electrons and some metal oxide, such as in zinc-manganese dioxide (Zn/MnO_2) alkaline battery. /6, 19/. In contrast, the electrons in metal-air batteries react directly with oxygen molecules that are obtained from the environment surrounding the cell. This oxygen reduction reaction (ORR) is what allows metal-air batteries to have many times the theoretical specific energy density of traditional batteries. During the discharge, oxygen molecules enter the cell along a diffusive cathode. The free electrons, which are transferred from the anode through an external circuit, initiate a reaction between these oxygen molecules and water molecules in the electrolyte to form hydroxide ions. These hydroxide ions can form hydroxide compounds with metal ions from the anode. /6, 12/

At the beginning of the reaction, in the electrolyte, there is an uneven concentration of different ions. The ions will then attempt to even this concentration difference via movement towards the area of low concentration. This is called diffusion. There is a continuous diffusion reaction occurring the in cell as result of oxidation reaction forming new metal

ions that will experience a pull towards the electrode with opposite charge. The movement of ions in the electrolyte due to the presence of the electric field in the cell due to different charges is referred to as migration. Besides diffusion and migration, the species might move through convection because of vibration or other external disturbance. /11, 17/

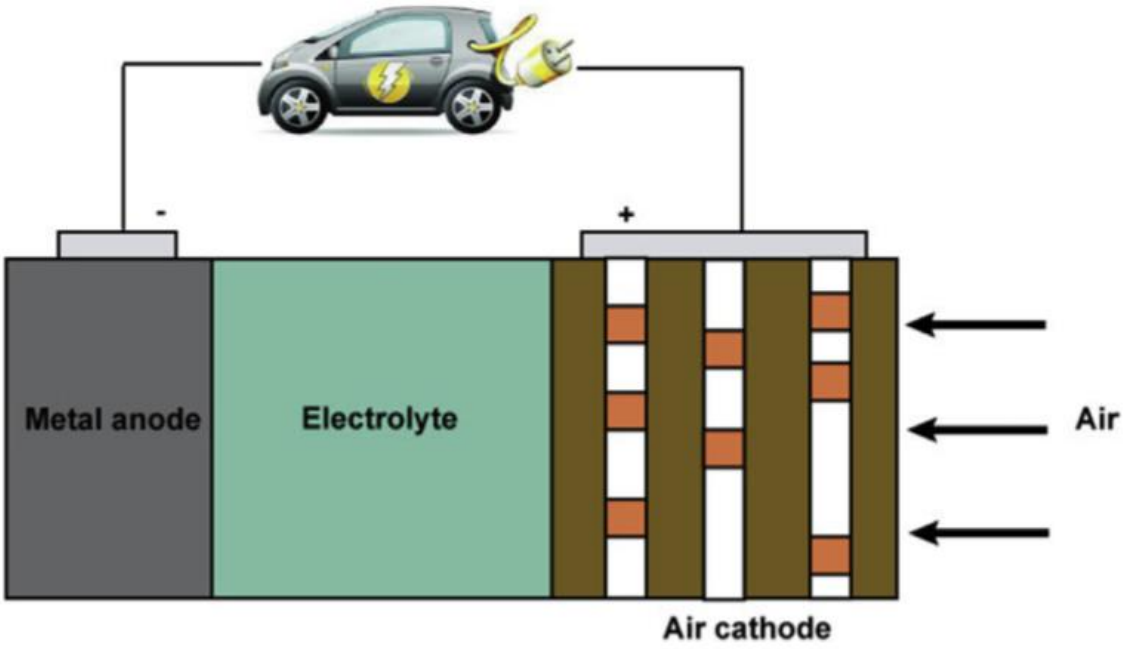

Figure 2. Functioning principle of metal-air battery /18/.

2.2 Structure

Researches have been interested in metal-air batteries with a plurality of chemistries to find the most practical system. As mentioned earlier the cell consists of three main components: an anode, a cathode and an electrolyte. The unique attribute of metal-air batteries is their open structure that is required to obtain air from the surrounding atmosphere. /10/. According to research, a combination of different metal compositions, catalysts and types of electrolytes have provided numerous challenges for a functional cell /15/.

2.2.1 Anode

The anode plays a critical role in the performance of metal-air batteries. A lot of research have focused on materials of different metal-compositions and purities to find an optimal anode composition. The choice of the anode material has an impact on the performance of the cell by enhancing the cell voltage and inhibiting the self-discharge. The discharge performance has been shown to be largely dependent on the type of anode material.

Therefore, the anode material should be chosen based on its position in electrochemical series, the formfactor of material and energy density. /20–21/

In an optimal anode, the metal that undergoes reaction, also called active material, should have as negative standard reduction potential (V) and as high Faradic capacity (Ah kg^{-1}) as possible. The capacity of the cell is determined by the amount of active material that takes part in the electron-transfer reaction. /19, 22/. The standard reduction potential (E°) tells the potential of the reduction reaction on the surface of the electrode, also called an interface, under standard conditions /17/. Standard conditions include temperature, pressure and the activity of the species. The standard reaction potentials are often listed with respect to the standard hydrogen electrode (SHE) which is set to 0 V. /23/

The important factors affecting the electrochemical performance of the anode electrode are found to be its morphology, purity and the contact surface area with the electrolyte. High-surface area materials, such as powder, flakes, ribbons and sheets, have been explored in many papers. The efficiency of each type of material is often linked to type of the electrolyte used. The overall performance of the anode is determined by the combined chemistry of the cell. /7, 11/

Common issues facing anode electrodes include metal degradation, hydrogen evolution reaction and formation of passivating film on the electrode. Research papers have shown that the effects of undesirable reactions can be reduced with correct selection of electrolyte and catalyst as well as reducing the amount of impurities in the anode. /11–12/

2.2.2 Cathode

The air cathode is a crucial component of the cell as it plays an important role in diffusion of oxygen, transfer of electrons and the oxygen reduction reaction. Ideally, it should have good electronic conductivity, high catalytic activity for ORR and be waterproof. The structure of the air cathode plays an important role in all these aspects. /13/. Research has shown that especially the thickness of the air electrode has an impact on the performance /6/. The typical composition of the air cathode comprises three main layers: the gas diffusion layer, current collector and catalytic active layer (Figure 3) /11, 15/.

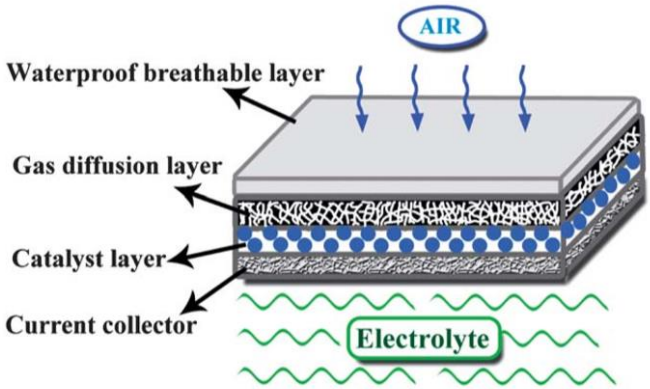

Figure 3. Typical cathode composition /11/.

The gas diffusion layer is composed of porous carbon material and hydrophobic binder that blocks water and only allows air to enter. /15/ The pore sizes in the material has shown to play huge importance in diffusion of the oxygen which affects the capacity of the battery. Too small pores have shown to suffer from becoming blocked easily while too large pores have shown to decrease the volumetric energy density of the battery (Wh m^{-3}). /6/ Some batteries also have shown to suffer from carbonation, which decreases the capacity and the life time of the battery, caused by carbon dioxide (CO_2) entering the system. To minimize the impact of CO_2 on the cell, it has been suggested to implement an absorption bed that would reduce the amount of CO_2 concentration in the cell. /10/

The primary purpose of current collector is to provide a low resistance path for current from one electrode to another. The current collector also influences the cell performance and can function as a substrate to reinforce other layers in the cathode. Metal mesh or foam are common choices for current collectors. /9/. Current collectors are often composed of nickel (Ni) /15/.

The catalytic active layer is where the ORR occurs. In many cases, systems use some type of catalyst to overcome sluggish reaction kinetics and reduce the overpotential. /10, 24, 25/. The catalytic active layer comprises carbon material, binder and the electrocatalyst. Typical catalysts are platinum (Pt), gold (Au), palladium (Pd) and silver (Ag). Platinum has been the most commonly used and has shown the best results while also being the most expensive. Due to the high cost of noble metals, use of alternative catalysts, such as transition metal oxides, have also been explored. /10, 12, 26/

2.2.3 Electrolyte

The electrolyte plays a vital role by providing a medium for the movement of ions which is essential for maintaining the reaction in the cell. Finding a correct type of electrolyte has proven to be one of the most challenging aspects of metal-air batteries. Research has suggested that electrolyte polarity and oxygen solubility are the most important factors affecting electrochemical performance. The type of electrolyte used depends on the overall chemistry of the cell as different metal-air batteries have different requirements for electrolyte. /6, 12, 18/

Electrolytes can be roughly categorized into four types: non-aqueous/aprotic, aqueous, hybrid and solid-state (Figure 4) /6, 10/. Aqueous systems are the simplest and most commonly used but they have limitations such as high corrosion rate and hydrogen evolution reaction. Non-aqueous, or aprotic type, electrodes are used in battery types where moisture could degrade the system for example in lithium-air battery, could create a fire or explosion hazard. In a typical hybrid structure, the anode's side is in contact with aprotic type electrolyte and cathode's side is in contact with an aqueous type of electrolyte. Ionic and gel based electrolytes are examples of non-aqueous electrolytes. /6, 10, 12/. On the downside, some non-aqueous electrolytes have raised safety concerns related to flammable organic solvents and are considered more expensive than aqueous types /15/. Totally solid-state electrolytes include polymer-ceramic and glass-ceramic materials /6/. They have shown high discharge potential, good rechargeability and thermal stability /6, 27/.

Some systems also include a separator which functions as an insulator that blocks transfer of unwanted ions, such as hydrogen ions for example. Common requirements for a separator include stability in alkaline electrolyte solution, inert to oxidation, proper pore size, high conductivity and electrically nonconductive. Common separators are polyethylene, polyvinyl alcohol (PVA) and polyethylene oxide (PEO). /6, 10, 18/

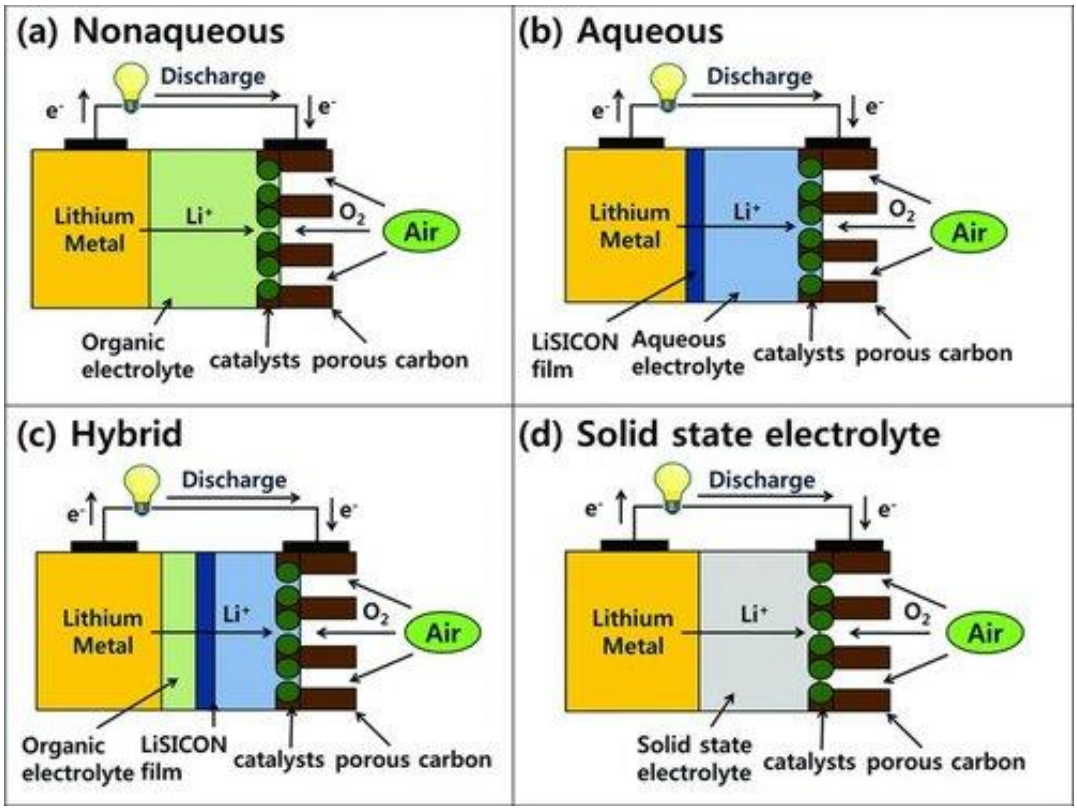

Figure 4. Schematics of Li-O_2 cells with different type of electrolytes: a) Aprotic/non-aqueous electrolytic type, b) Aqueous electrolytic type, c) Mixed type and d) Solid-state type /6/.

Many metal-air batteries have also suffered from issues related to electrolytes /29/. Aqueous types of electrolytes have especially been plagued with many problems. Common issues include anode degradations and corrosion, hydrogen evolution reaction and formation of passivating oxide film on the anode. Anode corrosion and degradation is a common issue with many anode metals, such as lithium and aluminium. /10, 15/. Anode degradation with aqueous type electrolytes has been tried to minimize by applying protective layers on the anode or using alloyed metals rather than pure metals /15, 24/. In some aqueous type of electrolytes, a parasitic reaction occurs, hydrogen evolution reaction, which results in accumulation of hydrogen gas /7/. The hydrogen gas is potentially explosive and can lower the capacity of the cell /10/. Aqueous electrolytes have also been known to evaporate at room temperature which changes the concentration of the electrolyte /6/. The formation of passivating oxide film is an issue particularly to aluminium and magnesium-air cells. The protective oxide film is a result of a spontaneous side reaction

that occurs when the anode is exposed to air and aqueous solutions. It leads to positive shift of the corrosion potential of the anode and slows down the anode activation. /10, 12/

3 MAGNESIUM-AIR BATTERY

As mentioned earlier, there are different types of metal-air batteries that are categorized according to metal used in anode electrode. The choice of anode material and the electrolyte will determine the attributes of the battery. The battery should have as high energy density and voltage as possible while also being environmentally friendly and cost efficient. Magnesium-air batteries have shown to hold great promise among the different types of metal-air batteries /7, 10–11/.

3.1 Introduction

Magnesium metal has been branded as an attractive candidate for metal-air batteries. Magnesium is the 8th most abundant element in the earth's crust and also common metal in sea water. As an anode material, it is extremely light metal (24.305 g mol^{-1}) and has high reaction activity which would make it an optimal choice for range extenders in electric vehicles. /10, 15, 23/. It has not only high theoretical gravimetric energy density (up to 6.8 kWh kg^{-1}) but also high theoretical cell potential (3.1 V) that is second only to that of lithium -air (3.4 V) /11, 15/. In contrast to lithium-air, it is environmentally friendly and safe to handle while lithium metal is toxic and provides fire and explosion hazard. /6,11/. Like many other metal-air batteries, Mg-air batteries have also shown to suffer from a huge drop between theoretical and operational voltage (Table 1) /15/. One of the key reason behind this is believed to be the corrosion of the magnesium anode /28/.

At present, Mg-air batteries have been largely considered only as primary batteries as current electrolytes prohibit Mg reversibility /29/. Rechargeable Mg-air batteries are under research but have so far demonstrated poor performance due to high overpotentials and limited cyclability /30–31/. While the primary Mg-air batteries cannot be recharged, the anode metal can still be mechanically replaced, making it refuellable /11, 15/. Magnesium-air batteries have been found especially attractive since they can potentially function as an underwater battery. In that case, the seawater, containing sodium chloride (NaCl), would function as an electrolyte and the oxygen would be obtained from oxygen absorbed in sea water. /32–33/

Mg-air batteries are still at their infancy stage and have been facing series of technical challenges such as corrosion of Mg, high self-discharge rate, short shelf life, sluggish

discharge kinetics and lack of rechargeability /15/. Numerous research papers have focused on understanding these issues /15, 33/.

3.2 Structure

Structure wise, Mg-air batteries are not different from other metal-air batteries. Common anode compositions consist of pure magnesium metal or magnesium alloyed with some other metals, such as zinc or aluminium. Alloying magnesium metal has been proven to reduce hydrogen evolution reaction, corrosion and in some cases, the particle size of the alloys. /11/. The magnesium anode has also been reported to suffer from self-discharge to which high surface area nanostructured magnesium alloys have been proposed as solutions /10/.

The air cathode has often been found to suffer from overpotential and high polarization during the oxygen reduction reaction which has led to decrease in cell performance. To compensate decreased performance, a lot of research has focused on developing a catalyst for neutral, acid and alkaline solutions. The most effective catalysts have been found to be noble metals, especially platinum, which, as downside, has also been found to be the most expensive solution. /11/. Research has also shown that a carbon fibre felt based cathode provides lower electrical resistivity and steadier structure than conventional carbon powder based cathodes used in Mg-air cells /13/.

A lot of research has focused on searching for the most suitable electrolyte for Mg-air batteries. Currently, the electrolyte is considered as one of the key reasons for the irreversibility of magnesium. /29/. Different kinds of electrolytes, such as aqueous, ionic and gel-based, have been proposed and tested and each type has shown its own benefits over other types. The most commonly investigated electrolytes are aqueous alkaline electrolytes, such as sodium chlorite (NaCl), potassium hydroxide (KOH) and sodium nitrate ($NaNO_3$) solutions. Drawbacks of many aqueous electrolytes have been evaporation of the electrolyte, corrosion and formation of protective oxidation film on the electrode that leads to anode passivation. However, alkaline aqueous solutions have shown higher resistance to corrosion and hydrogen evolution reactions than neutral or acid solutions. /11/. The use of ionic and gel type electrolytes has also been proposed to minimize the issues

with aqueous solutions. Commonly researched ionic electrolytes include trihexyl(tetradecyl)phosphonium dicyanamide ([$P_{6,6,6,14}$][DCA]) and tributyl(decyl)phosphonium chloride ([$P_{6,6,6,10}$][Cl]). /10, 29/

3.3 Reaction Mechanism

The reaction mechanism of Mg-air cell can differ according to the number of steps in the reaction. Typically, in the oxidation half-reaction, the magnesium atoms in the anode release two electrons and become magnesium ions with positive charge (equation 2). /11/

$$Mg \rightarrow Mg^{2+} + 2e^- \quad (2)$$

In the reduction half-reaction, the free electrons from the anode initiate reaction between oxygen molecules and water molecules in the electrolyte to form hydroxide ions (equation 3) /11/.

$$O_2 + 2H_2O + 4e^- \rightarrow 4\,OH^- \quad (3)$$

The overall reaction consists of both half-reactions which results in the formation of magnesium hydroxide (equation 4) /11/.

$$2Mg + 2H_2O + O_2 \rightarrow 2Mg(OH)_2 \quad (4)$$

However, magnesium anode is known to suffer from parasitic reactions in the presence of aqueous electrolytes, such as corrosion reaction, that leads to decrease in the faradaic efficiency of the cell. The effects of parasitic corrosion in oxidation and corrosion reactions can be described with the following equations (equations 5–7). /33/

$$Mg \rightarrow Mg^{2+} + 2e^- \quad (5)$$

$$2H_2O + 2e^- \rightarrow H_2 + 2OH^- \quad (6)$$

$$Mg + 2H_2O \rightarrow H_2 + Mg(OH)_2 \quad (7)$$

4 COMPOSITION OF THE BATTERY

4.1 The Components

The modelled battery consists of a simple cell composition of an anode, a cathode and an electrolyte as shown in Figure 5. Pure magnesium metal was chosen as an anode material due to its high corrosion resistance /11/. Cast metal was chosen over powder due to it allowing a thinner electrode /34/. The anode has dimension of 5 × 0.12 cm and comprises 1 g of active material. Figure 6 shows a scanning electrode microscope (SEM) image of the magnesium anode which depicts magnesium particles with the mean size of 300 nm /35/. The anode is connected to the cathode via a current collector.

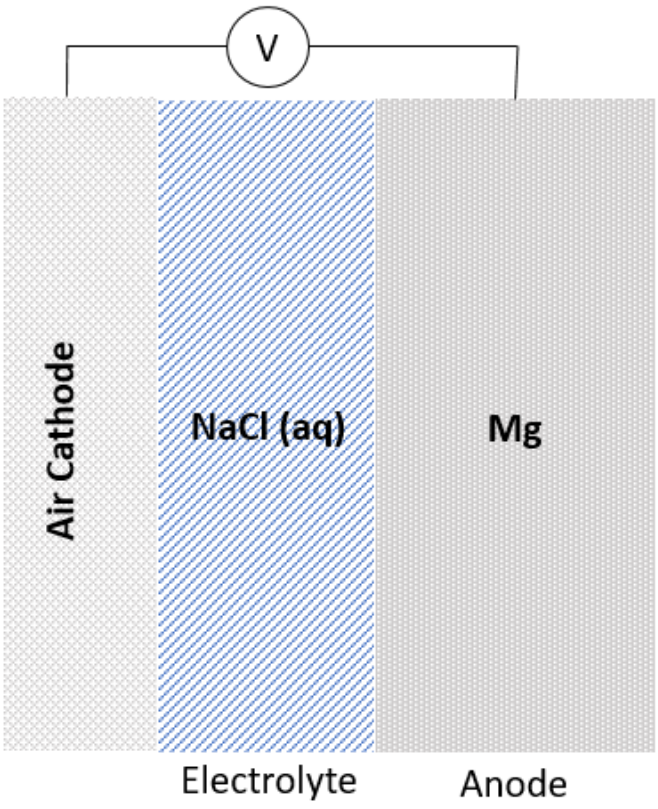

Figure 5. Schematic of the Mg-air cell.

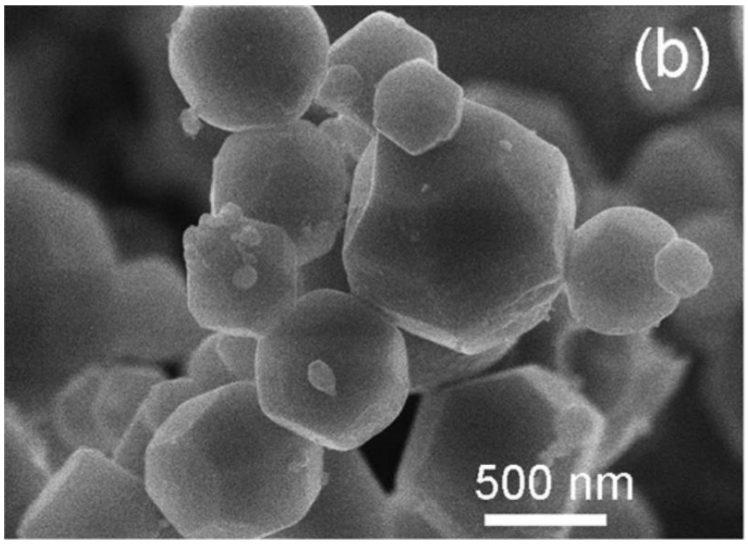

Figure 6. SEM image of the magnesium anode /35/.

An aqueous NaCl-solution was chosen as an electrolyte. The choice was based on large amounts of data available for simulation and ease of synthetizing. On the downside, it suffers from parasitic reactions which are not taken into account in this thesis /10/.

A carbon fibre felt based cathode was chosen as a cathode due to its favourable results in experiments published in papers. Especially the stability and performance of the carbon fibre cathode has shown great improvement over carbon powder based cathode. **Figure 7** depicts scanning electron microscope image of the cathode. /13/

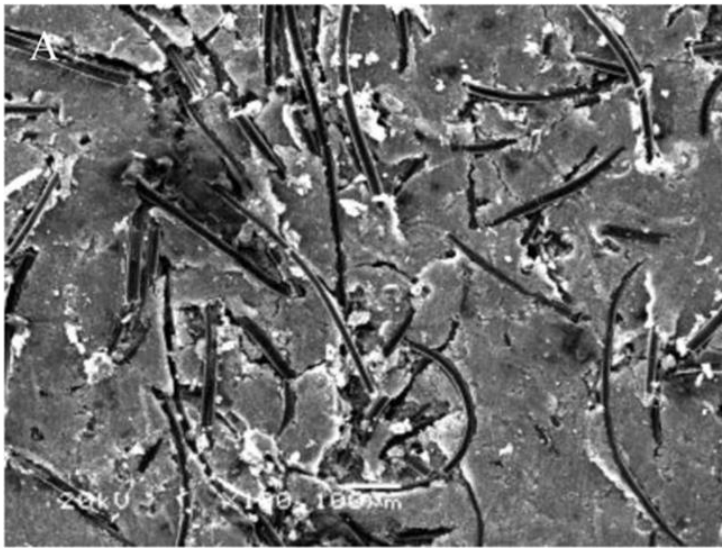

Figure 7. SEM image of carbon fibre felt cathode /13/.

4.2 One Step Reaction

In this thesis, the one step reaction was chosen to simplify the reaction mechanism. The redox-reaction begins once the potentials of the electrodes reach -2.69 V and 0.40 V (**Figure 8**). A standard hydrogen electrode (SHE) is used as a reference electrode. In the one step reaction, the magnesium metal reacts directly with hydroxide ions in the electrolyte to form magnesium hydroxide (equation 8). At the cathode, the hydroxide ions are formed in the reaction between the free electrons, oxygen and water molecules (equation 9). The overall reaction consists of both half-reactions with overall standard cell potential of 3.09 V (equation 10). /10/

$$2Mg + 4OH^- \rightarrow 2Mg(OH)_2 + 4e^- \qquad E° = -2.69 \text{ V vs. SHE} \qquad (8)$$

$$O_2 + 2H_2O + 4e^- \rightarrow 4\,OH^- \qquad E° = 0.40 \text{ V vs. SHE} \qquad (9)$$

$$2Mg + 2H_2O + O_2 \rightarrow 2Mg(OH)_2 \qquad E_{overall} = 3.09 \text{ V vs. SHE} \qquad (10)$$

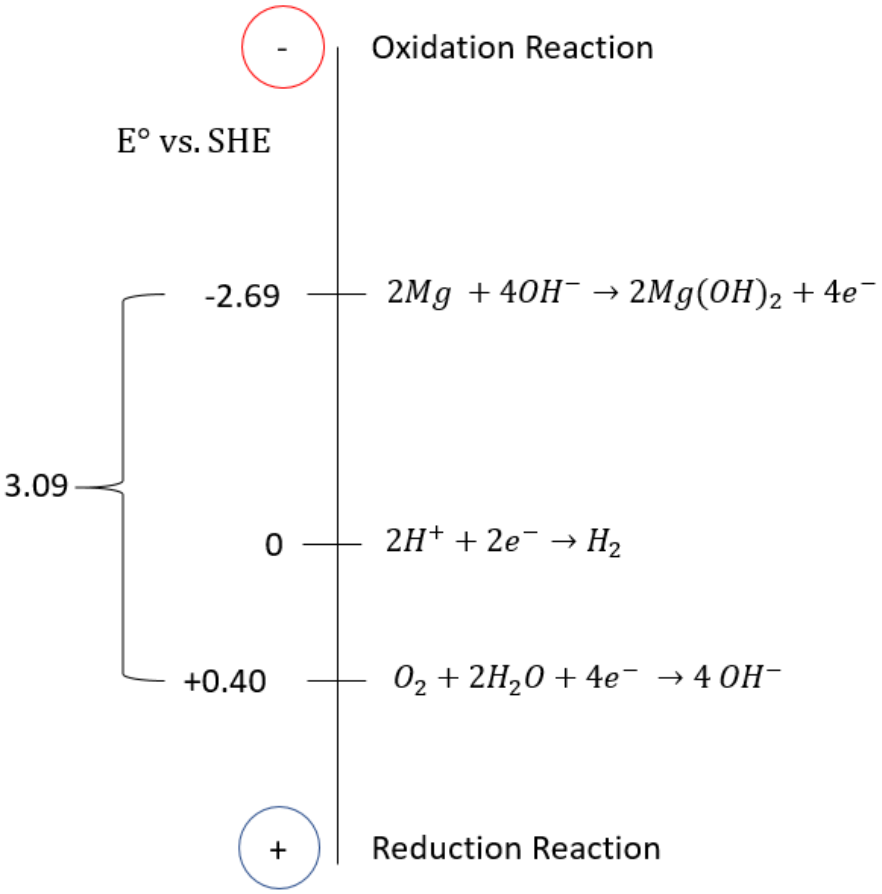

Figure 8. The reaction potentials with respect to standard hydrogen electrode.

5 GOVERNING EQUATIONS

The governing equations describe the essential behaviour of the system. They include mathematical descriptions of the interactions between the magnesium anode electrode, electrolyte and the air cathode. These interactions will result in a output of electrical energy. The governing equations are divided into two sets of equations: mass balance and electrochemical kinetics. The mass balance equations are based on the law of conservation of mass which states that matter can neither be destroyed nor created /36/. The electrochemical kinetics on the other hand, are a set of equations that describe the electrode-electrolyte interactions /17/.

5.1 Assumptions

Following assumptions were made in this model:

- The model is two-dimensional.
- The reaction mechanism is considered as one step reaction from Mg to $Mg(OH)_2$.
- The temperature of the cell and the surrounding environment stay constant throughout the discharge.
- The rate of anodic reaction is assumed.
- Transport of species in the electrolyte is diffusion limited.
- Convection of the species is neglected.
- System is not limited by oxygen reaction.
- Parasitic reactions are neglected.
- The discharge process is continuous.

The assumptions provide the necessary simplifications to focus on the key factors affecting the performance of magnesium-air cell. The model is assumed two-dimensional due to simplifications. The complicated reaction kinetics caused by the multistep mechanism is neglected with the one step reaction mechanism. The model is simplified by assuming the discharge process continuous, during which no parasitic reactions take place. Assuming an unlimited supply of oxygen in constant temperature eliminates the risk of reaction failure during the discharge. The model is further simplified by assuming that no vibrations occur inside the cell and that the transport of species is diffusion limited. Finally,

the rate of anodic reaction was assumed based on performance expectations due to lack of directly applicable data.

5.2 Mass Balance

5.2.1 Nernst-Planck Equation

One of the most essential set of equations are mass transfer equations which describe the movement of matter from one location inside the cell to another. Mass transfer plays an important role in electrochemical dynamics. Without mass transfer, the cell reactions cannot be sustained. There are three types of mass transfer: diffusion, which occurs due to concentration differences; migration, which is movement of ions due to electric field created by charges; and convection, which occurs due to vibrations or stirring. /16–17/. The general mass transfer in two-dimensional Cartesian space $\mathbb{R}^2$ can be described mathematically by a differential equation called the Nernst-Planck equation (equation 11) /16/.

$$J(x,y,t) = -D\frac{\partial C(x,y,t)}{\partial x \partial y} - \frac{zFDC}{RT}\frac{\partial \phi(x,y,t)}{\partial x \partial y} + C(x,y,t)V(x,y,t) \qquad (11)$$

The Nernst-Planck equation includes all three modes of mass transport, the first term on the right-hand side is diffusion term, the second term is migration and the third term is convection. Together, they result in the rise of flux. In the equation, J stands for the flux (mol m^2 s^{-1}) at time t in x and y directions, D is the diffusion coefficient, $\partial C/\partial x \partial y$ is the concentration gradient, z stands for the charge of the electroactive species, F is the Faraday's constant (96,500 C mol^{-1}), R is the gas constant (8.31 J K^{-1} mol^{-1}), T is the constant temperature of the cell (298.15 K), $\partial \phi/\partial x \partial y$ stands for the electrical gradient imposed by the charges inside an electric field and V stands for hydrodynamic velocity. /16, 23/

5.2.2 Diffusion

Diffusion is movement of species due to the concentration gradient. The concentration difference inside the cell creates a flux of material flowing towards the end with lower concentration, resulting in a decrease of concentration difference. The concentration gradient points in the direction where the change in concentration is highest. The material moves between the surface of the electrode, also called an interface and a bulk solution which is a location farther away from the electrode in the electrolyte. /16–17/

When magnesium ions react with hydroxide ions on the interface, they form magnesium hydroxide. Consequently, the formation products start to precipitate in the electrolyte. This creates a concentration difference on the interface which leads to the generation of a concentration gradient adjacent to the interface. This in turn, gives a rise in diffusional flux towards a region of lower concentration (Figure 9). The rate of diffusion can be described mathematically by the Fick's first law of diffusion (equation 12). According to the Fick's first law, the diffusional flux is directly proportional to the slope of the concentration gradient. The concentration gradient is negative as it is pointing in the direction where the amount of concentration decreases the most. /16–17/

$$J(x,y,t) = -D\nabla C = -D\frac{\partial C(x,y,t)}{\partial x \partial y} \tag{12}$$

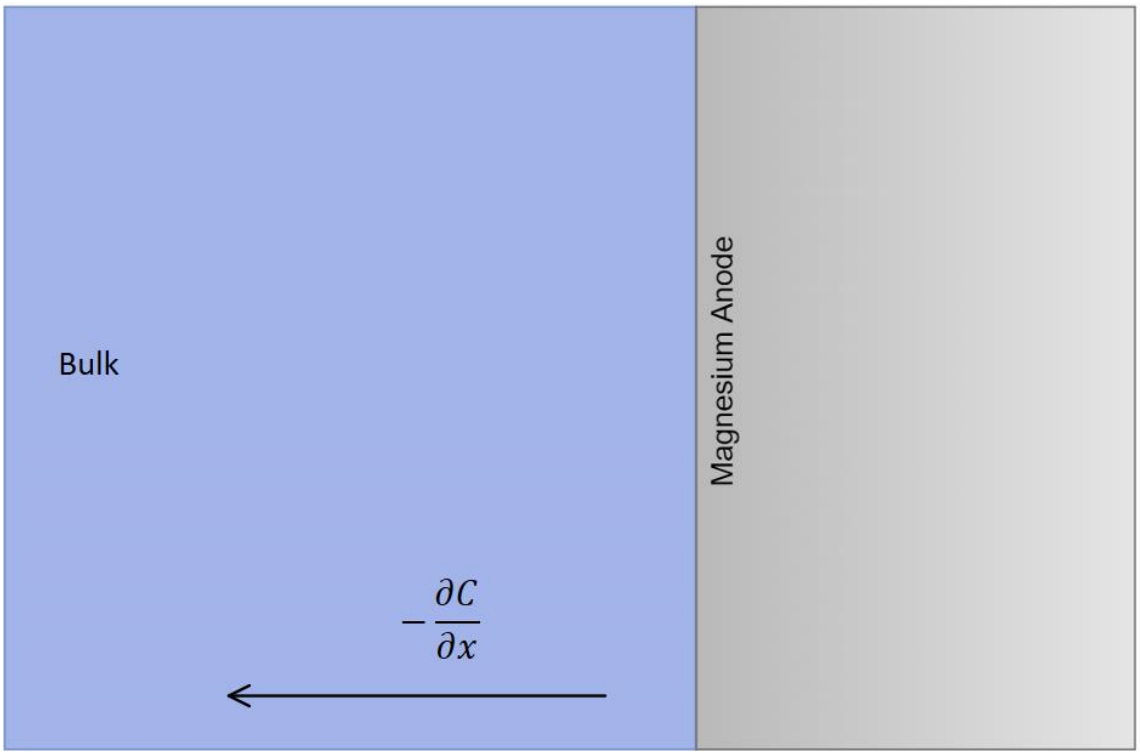

Figure 9. The concentration gradient at the interface.

5.2.3 Migration

Migration describes a movement of ions in the electrolyte under the influence of electric gradient. Ions, with different electric charge, experience the Coulomb's force pulling them towards opposite charges in an electric field created by the charges inside the cell. The effects of migration are stronger in the bulk solution where the concentration gradient

is much smaller. The movement of ions between the two electrodes are illustrated in Figure 10. The flux created by migration can be described mathematically by equation 13. /16, 17/

$$J(x,t) = -\frac{zFDC}{RT}\frac{\partial\phi(x,y,t)}{\partial x \partial y} \tag{13}$$

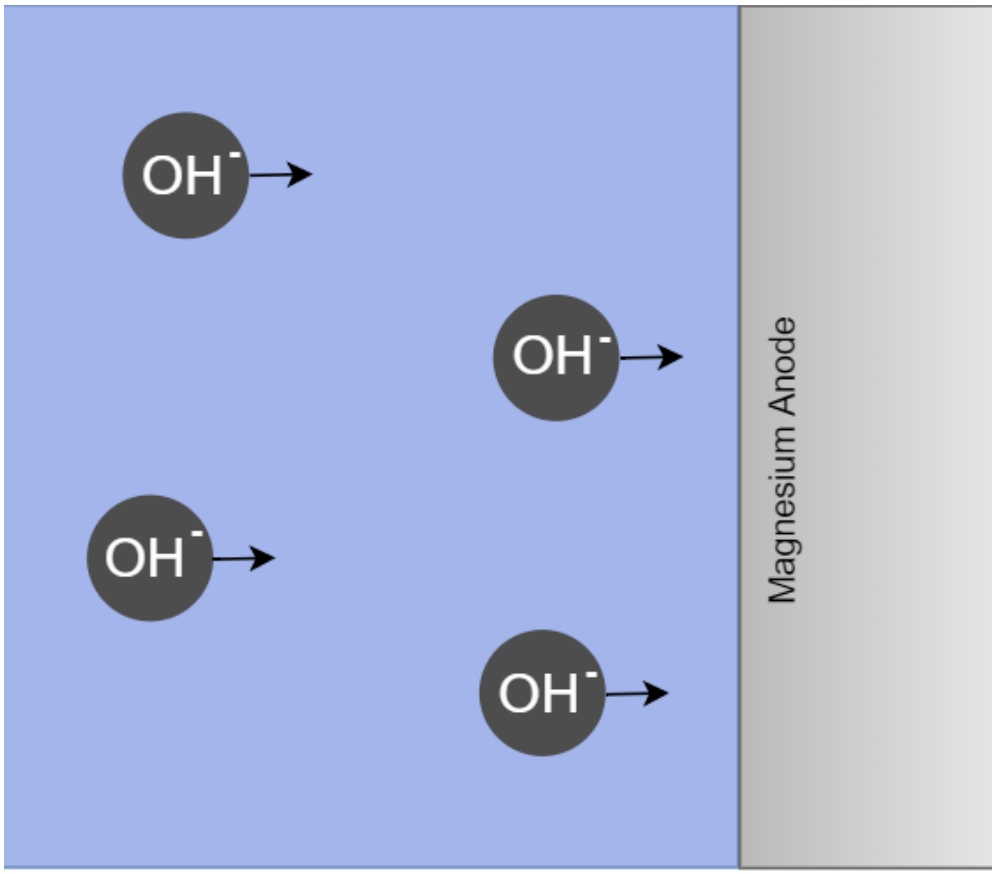

Figure 10. The movement of ions caused by the electric gradient.

5.2.4 Convection

The 3rd mode of mass transport is convection. Convection describes the movement of mass in a fluid that is caused by an imbalance of forces on the solution. The physical movement of species can occur as a result of forced convection, such as stirring or vibration of the electrode, or due to naturally occurring convection caused by density differences in the solution. /16/. In the presented model, it is assumed that there are no vibrations occurring inside the cell, however, it is described as:

$$J(x,y,t) = C(x,y,t)V(x,y,t) \tag{14}$$

5.2.5 Mass-Transport Limitation

Mass balance is a step-determined reaction that consists of multiple different steps with different modes of mass transfer. The rate of flux is determined by the slowest step in the reaction kinetics. /16/. The mass transportation is most often assumed to be controlled either by diffusion or migration /16, 37/. It is widely accepted that metal-air batteries suffer from diffusion limitation. Diffusivity and concentration of the dissolved oxygen have been shown to limit the performance of the cell, especially with high current densities. /38–41/. In this model, the mass transfer is assumed to be diffusion-limited.

5.3 Electrochemical Kinetics

5.3.1 Gibbs Free Energy

As mentioned earlier, the Mg-air battery functions as a galvanic cell during the discharge. Chemical reactions in a galvanic cell occur spontaneously when the change in Gibbs free energy of the system remains negative /17/. The Gibbs free energy describes the amount of chemical energy in the cell that can be converted into electrical energy /19/. This thermodynamic relationship between spontaneous cell reaction and Gibbs free energy is described in equation 15. In the equation, ΔG stands for the change in free energy, n is the number of exchanged electrons in the reaction, F is the Faraday's constant that describes charge on a mole of electrons and $E°$ is the standard potential (V). The negative free energy represents energy conversion by the system due to cell reactions. /10, 17/

$$\Delta G = -nF\mathrm{E}° \tag{15}$$

5.3.2 Faradaic and Non-Faradaic Processes

In general, there are two types of processes occurring at the electrodes: Faradaic and non-Faradaic processes. Faradaic processes include all chemical reactions that are governed by the Faraday's law, such as redox-reactions. The Faraday's law states that the amount of electrochemical changes in an electrode is proportional to the quantity of charge passed and thus the faradic current can be used as a measure of redox reaction. These reactions are also called charge-transfer reactions and the electrodes in which they occur, charge-transfer electrodes. The charge-transfer reaction occurs within certain potential range where the reaction is thermodynamically favourable. /16–17/. In case of the modelled

battery, the range is from -2.69 V to 0.40 V with respect to standard hydrogen electrode (**Figure 8**) /10/.

Because the system is governed by the laws of thermodynamics, its potential under non-standard conditions can be found with the Nernst equation (equation 16). The Nernst equation describes electrode potential as a function of concentration. Due to electrode reactions, there is a constant change in concentration which leads to a change in the potentials of electrodes. In the Nernst equation, *E* is the potential under non-standard conditions, *E*° stands for standard potential, *R* stands for gas constant, *T* is the temperature of the cell (298.15K), n is the number of electrons involved in the reaction, *F* stands for the Faraday's constants and C_O and C_R are oxidation and reduction species concentrations during the reaction. /16–17/

$$E = \mathrm{E}^\circ - \frac{RT}{nF} ln \frac{C_O(0,t)}{C_R(0,t)} \tag{16}$$

Non-faradaic processes occur through adsorption and desorption processes which alter the structure of the electrode surface. Consequently, this results in decrease in electrode potential and solution composition. Polarization is an essential non-faradaic process which lowers the potential of the battery. In polarization, electrode potential deviates from equilibrium potential upon passage of Faradaic current. The extent of polarization is described with overpotential. It can be viewed as less negative potential at the anode and less positive potential at the cathode. Overpotential, caused by polarization, can be divided into two types: activation overpotential, which occurs at the initial stages of discharge; and concentration polarization, which occurs at the end of discharge. The activation overpotential describes the amount of activation energy required to drive the electron-transfer reaction. The concentration overpotential on the other hand, describes the amount of activation energy required for the mass transfer to maintain the electron-transfer reaction at the end of discharge. Overpotential can be described mathematically as the difference between real potential and equilibrium potential, which describes the potential when the net movement of charged particles is 0 (equation 17). In the equation, η stands for overpotential, *E* is potential under non-standard conditions (equation 16) and E_{eq} is the equilibrium potential. /17/

$$\eta = E - E_{eq} \tag{17}$$

5.3.3 Activation Energy Barrier

Reactions in the cell require a certain amount of potential energy to proceed. In a redox-reaction (equation 1), the electrodes must overcome the energy barrier for electron transfer. The reason for this lies within the different structures of the reduction and oxidation agents which leads to the formation of an energy barrier of Gibbs free energy. The energy requirement to overcome this barrier is called activation energy. /16–17/. Generally, the frequency with which the electron crosses the activation energy barrier, the rate of reaction, can be described with the Arrhenius equation (equation 18). The Arrhenius equation is an empirical generalization of the relationship between the temperature and the rate of reaction,

$$k = Ae^{-\frac{E_a}{RT}} \tag{18}$$

where k (s^{-1}) is rate constant, which describes the rate of reaction at set temperature; A (s^{-1}) is frequency factor, which describes the frequency of attempts to surmount the energy barrier; E_a is the activation energy (kJ mol^{-1}) of the species which the system needs to overcome in order for reaction to occur; R is the gas constant; and T is the temperate of the cell. /16–17/

5.3.4 Electron-Transfer Reactions

As has been mentioned earlier, redox-reactions are controlled by the rate of electron transfer. However, the redox-reaction only occurs while there are sufficient mass transport reactions in the cell. Other factors that influence the electron transfer are polarization due to the change in concentration during the reaction, formation of passive film and hydrogen evolution reaction. /11, 16–17/. Due to the simplification of the model, only the effects of polarization are taken into account.

In the system, there are two kinds of electron-transfer reactions: the forward or anodic reaction and backward or cathodic reaction. The electron-transfer reactions involve the transfer of electron between the electron orbital of oxidation or reduction products and the electrodes. Simultaneously, both reactions create forward and backward currents. The difference between forward and backward current is the net current (A) of the system (equation 19). /16–17/

$$i_{net} = i_f - i_b \tag{19}$$

The net current requires a deviation from equilibrium potential to overcome the activation energy to drive mass transfer reactions. A large positive overpotential accelerates the movement of charge to the anodic direction and vice versa. If there exists no overpotential to unbalance the anodic and cathodic currents, the net current is zero. Despite not having the net current flowing, there is still a continuous movement of charge carriers in a way that faradaic activity is balanced. The movement of charge particles in this manner is called the exchange current (i_o), which has the magnitude of either forward or backward current (equation 20). /16–17/

$$i_o = i_f = i_b \tag{20}$$

The exchange current can be thought as a measure of the ability of a cell to deliver the net current without significant losses across the electrode-electrolyte interface /17, 42/. It is often normalized to a unit of area and called the exchange current density (A m^{-2}). /17/. The relationship between the current density produced by electron-transfer reaction and overpotential can be described with the general Butler-Volmer equation (equation 21),

$$i_j = i_o(e^{\frac{-\beta nF\eta}{RT}} - e^{\frac{(1-\beta)nF\eta}{RT}}) \tag{21}$$

where i_j is the current density, i_o is the exchange current, β is the charge transfer coefficient (0.5) that is a measure of symmetry of the activation energy barrier, n is the number of electrons involved in the reaction, R is the gas constant, F is the Faraday's constant and η is the overpotential (equation 17) /17, 42–43/.

The Butler-Volmer equation describes the exchange current density for normal redox couples as a function of overpotential. It consists of both forward and backward reactions. The first half of the equation describes anodic current density caused by forward reactions and the other half by backward reactions. Both anodic and cathodic reactions follow Arrhenius-type kinetics (equation 18). /17, 42/

Based on the electron-transfer reaction, the cell capacity is calculated according to equation 22, where C_{ah} stands for the cell capacity, i_{load} is the discharge current, Δt is the discharge time and m is the mass of the active material /19/

$$C_{Ah} = \frac{i_{load} \cdot \Delta t}{m} \tag{22}$$

5.4 The Sink Term

As mentioned earlier, the rise in the diffusional flux towards the region of lower concentration can be described mathematically by the Fick's first law (equation 12). However, the precipitation of $Mg(OH)_2$ is not an isolated process but is connected to the reactions in the anode. This connection between electrolyte and anode reactions is established with the sink term. The sink term describes the rate of electrochemical reactions in the electrolyte according to the reactions in the anode, described by Butler-Volmer theory (equation 21). The sink term can be described mathematically by equation 23, where *a* is the area of the electrode surface that is facing the reaction, i_j is the electrode current density described by the Butler-Volmer equation (equation 21), *n* is the number of electrons involved in the reaction and *F* is the Faraday's constant. /44/

$$S = -\frac{a i_j}{nF} \tag{23}$$

However, the change in concentration does not only occur over the change in distance but through time as well. As a result, the Fick's second law can be used to predict and model change in concentration through time. The Fick's second law, combined with the sink term, can be described by following the second order non-homogeneous partial differential equation (equation 24). In the equation, the S stands for the sink term. /16–17/

$$\frac{\partial C(x,y,t)}{\partial t} = -D\frac{\partial^2 C(x,y,t)}{\partial x^2 \partial y^2} + S \tag{24}$$

The whole process of diffusion in the electrolyte, with respect to the anodic reactions, can be described numerically by the following equation (equation 25) /43/.

$$\frac{\partial C_{i,x}}{\partial t} = \sum_{j}^{neighbours} D(c_{j,x} - c_{i,x}) + S \tag{25}$$

The equation has three boundary conditions: time at the beginning, time at the end and the size of the element. In the equation, $c_{j,x}$ is the concentration of species *x* ($Mg(OH)_2$)

at a point in the electrolyte and $c_{i,x}$ is the concentration of species at a neighbouring point. /43/

6 METAL-AIR BATTERY SIMULATION

6.1 Methodology and Tools

6.1.1 Parameters

Table 2 shows the parameters that were used in the simulation. The dimensions of the cell components are shown in Figure 11.

Table 2. Parameters used in the simulation.

Parameter	Symbol	Value	Unit	Reference
		Structural parameters		
Height of the anode	a	5×10^{-2}	m	Assumed
Width of the anode	x_a	12×10^{-4}	m	Calculated
Mass of the anode	m	1	g	Assumed
Density of Mg	ρ	1.74	g m^{-3}	/23/
		Reaction parameters		
Standard potential of the anode	$E°_{anode}$	2.69	V	/10/
Standard potential of the cathode	$E°_{cathode}$	0.4	V	/10/
Diffusion coefficient	D	0.7×10^{-10}	m^2 s^{-1}	/45/
Rate of reaction	k^o	3.42×10^{-7}	m s^{-1}	Assumed
Gas constant	R	8.31	J K^{-1} mol^{-1}	/23/
Temperature	T	298.15	K	Assumed
Faraday's constant	F	96,500	C mol^{-1}	/46/
Charge transfer coefficient	β	0.5	-	/17/
Concentration of Mg	C_{Mg}	1	mol dm^{-1}	Assumed
Concentration of $Mg(OH)_2$	$C_{Mg(OH)2}$	1	mol dm^{-1}	Assumed
Concentration of O2	C_{O2}	1	mol dm^{-1}	Assumed
Concentration of OH	C_{OH}	1	mol dm^{-1}	Assumed

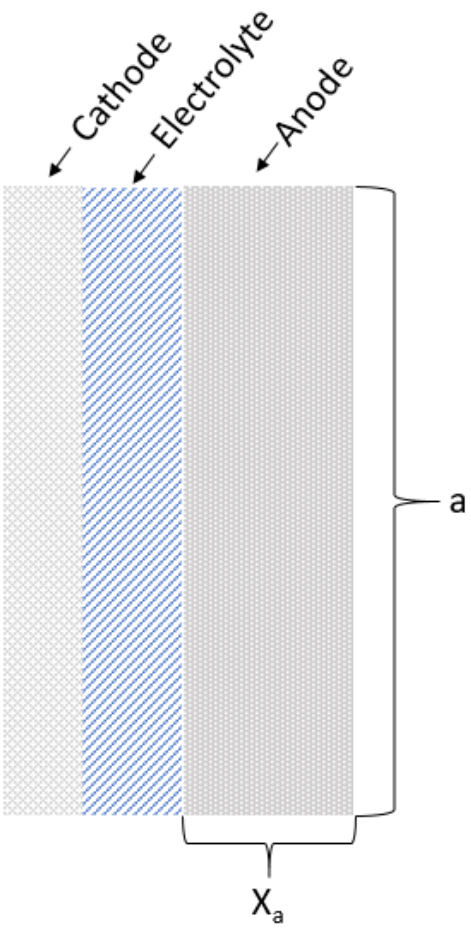

Figure 11. The schematic of the cell with dimension.

6.1.2 Numerical Methods

The mathematical model was implemented using numerical methods. Many real-life problems are extremely complex and nonlinear in nature, which would make them extremely difficult, or even impossible, to solve precisely using analytical methods. Numerical methods are used to model and solve complex mathematical problems in science and engineering by approximating a solution. Many numerical methods are largely done with the help of computers due to the large quantity of algebraic calculations involved. /47/.

In this model, the partial differential equations were solved using the finite element method. In the finite element method, the complex object (domain), which is being modelled, is discretized into smaller segments (finite elements). The boundary conditions and continuous differential equations are then applied to the elements to find the approximate solution. /48/

6.1.3 Flow Chart

Figure 12 shows the flow chart of the simulation. The active surface area of the electrode, applied load current density and species transport in the electrolyte are inputs. The next step includes the governing equations: the electrochemical kinetics and mass balance. The final step is the cell potential, after which the simulation ends.

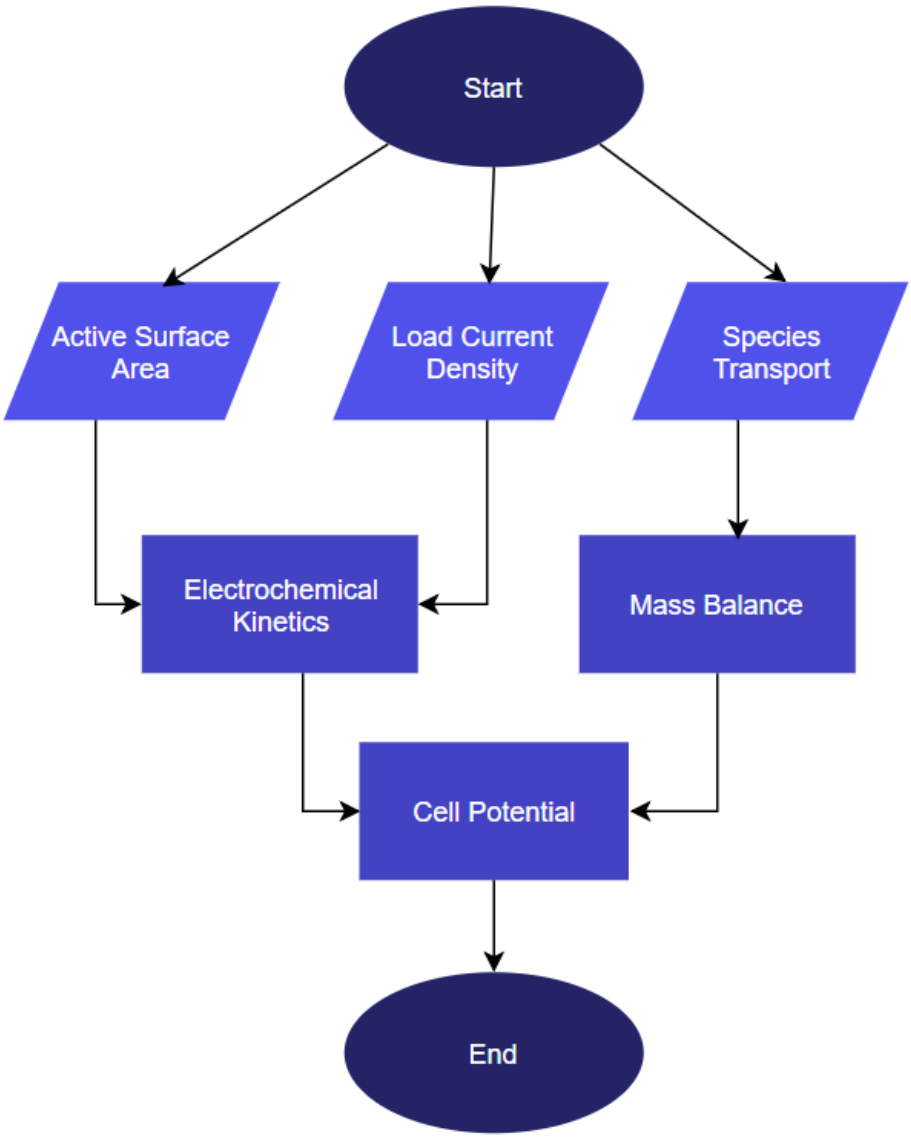

Figure 12. The flow chart of the simulation

6.1.4 The Simulation

The two-dimensional simulation was developed using the Python 3 programming language. Python 3 is an object-oriented programming language that can be used to develop

engineering applications. It is an interpreted language which makes testing, debugging and running the code fast. /49/. The main libraries used in this simulation were NumPy, which provided the necessary code packages for scientific computing and Matplotlib, which is a collection of plotting functions. Spyder was used as an integrated development environment (IDE) that integrates different libraries and the IPython interpreter, which runs the code, into one application /50/.

Besides Python, OVITO was used to visualize the anode reaction. The Open Visualization Tool (OVITO) is an open-source 3D visualization and analysis software for atomistic and particle simulation data /51/.

7 RESULTS & DISCUSSION

7.1 Anode Electrode

Initially, the anode consists of pure magnesium. During a discharge, the magnesium (Mg) reacts with the hydroxide ions (OH^-) in the electrolyte and forms magnesium hydroxide ($Mg(OH)_2$), as described in equation 8. This leads to a precipitation of $Mg(OH)_2$ which causes changes in the morphology of the electrode. As mentioned earlier, the reaction results in increasing overpotential (equation 17). Because of this, the potential of the anode electrode decreased during the simulated discharge. Figure 13 represents voltage-time curve of the Mg anode as a result of those reactions.

In the graph, the blue curve represents the anodic potential during the discharge. The discharging is carried out with load current density of 1 A m^{-2}. The discharge time of the cell is represented as a function of cell potential. The duration of the discharge was short due to a small amount of active material (1 g) in the anode. At the initial stages of discharge, the anodic potential was in steady decline. This was due to alteration in the morphology of the anode as a result of overpotential. The anodic potential dropped sharply at the end as the electrode approached depletion of active material.

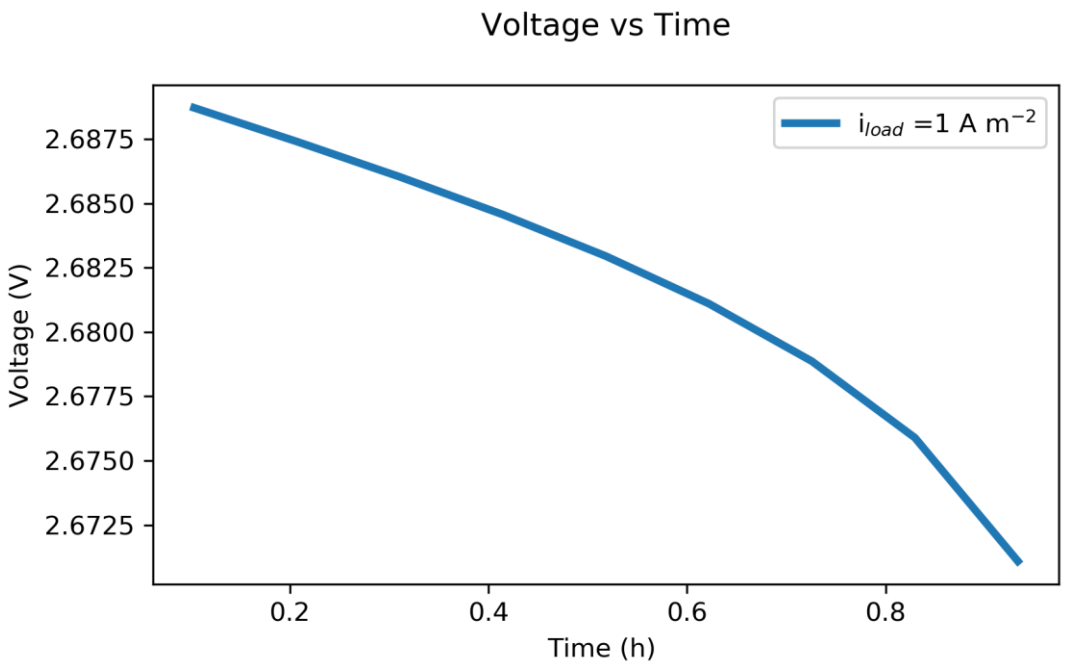

Figure 13. The anodic potential.

Figure 14 illustrates a 3D visualization of the magnesium anode during different stages of the discharge process. It was done using the Open Visualization Tool (OVITO). The black particles illustrate elemental magnesium which, during the redox-reaction, form magnesium hydroxide, represented with blue colour. The images on the voltage-time curve represent the anode on different stages of discharge. Together, the Figure 13 and Figure 14 further emphasize the connection between the rate in drop of anode potential and the stage of depletion of magnesium. The rate of potential drop is lower at the beginning of the discharge as there were only small changes in the morphology. As the reaction proceeded, the consumption of active material had caused further alteration to the morphology of the electrode. Hence, a higher overpotential was required to maintain the electron-transfer reaction, which showed as a higher potential drop.

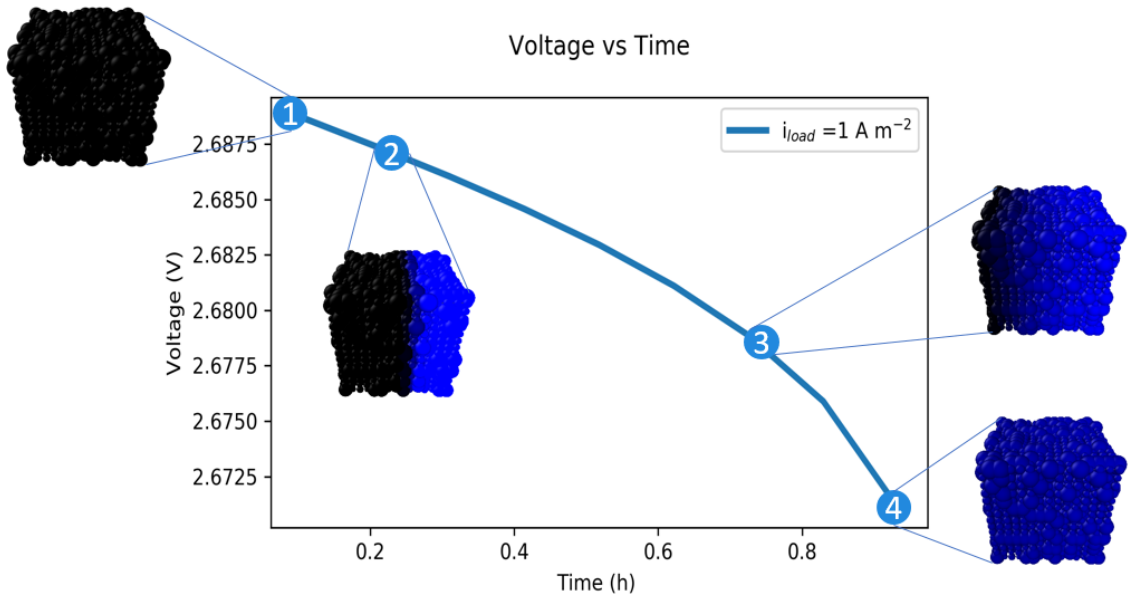

Figure 14. The magnesium anode during different states of discharge: 1) in state of full charge, 2) after 0.2 hours, 3) after 0.7 hours, d) in state of full discharge.

According to the Butler-Volmer theory (equation 21), the electrode current density is obtained as a function of overpotential. As a result, the growing overpotential at the anode led to increase in anodic current density. This relationship between the anodic potential and current density is shown in Figure 15. The graph also demonstrates the activation energy barrier of the magnesium anode. In order for the reaction to occur, the anode has to reach the activation potential which can overcome the activation energy barrier of Gibbs free energy. As seen on the graph, the electron-transfer reaction started once the

anode reached the potential of 2.69 V (vs. SHE). The overpotential created a shift in the anodic potential from the equilibrium value towards positive direction. As the overpotential continued to increase, the anodic current also increased, as predicted by the Butler-Volmer equation.

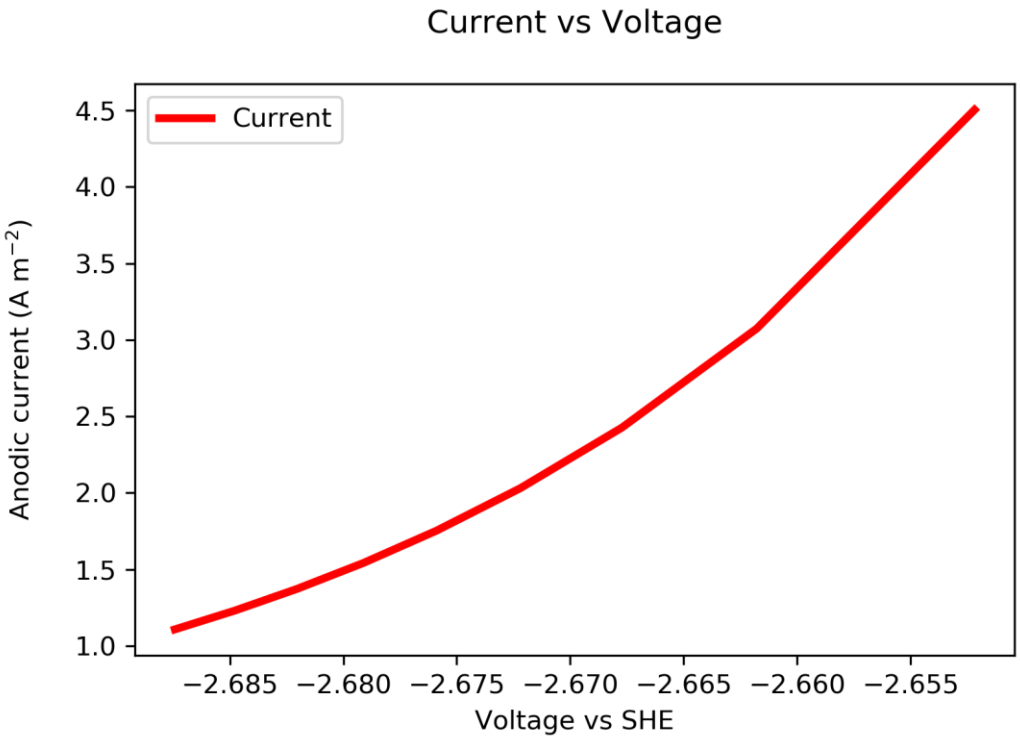

Figure 15. Anodic potential vs current.

7.2 Cathode Electrode

Similarly, the reduction reaction caused a change of species at the cathode led to a decrease in cathodic potential during the discharge as shown in Figure 16. The shape of the cathodic potential curve is identical to the anodic counterpart. The potential curve declined steadily until the end, when there was a large drop in potential. The discharge time is also identical to the anodic reaction.

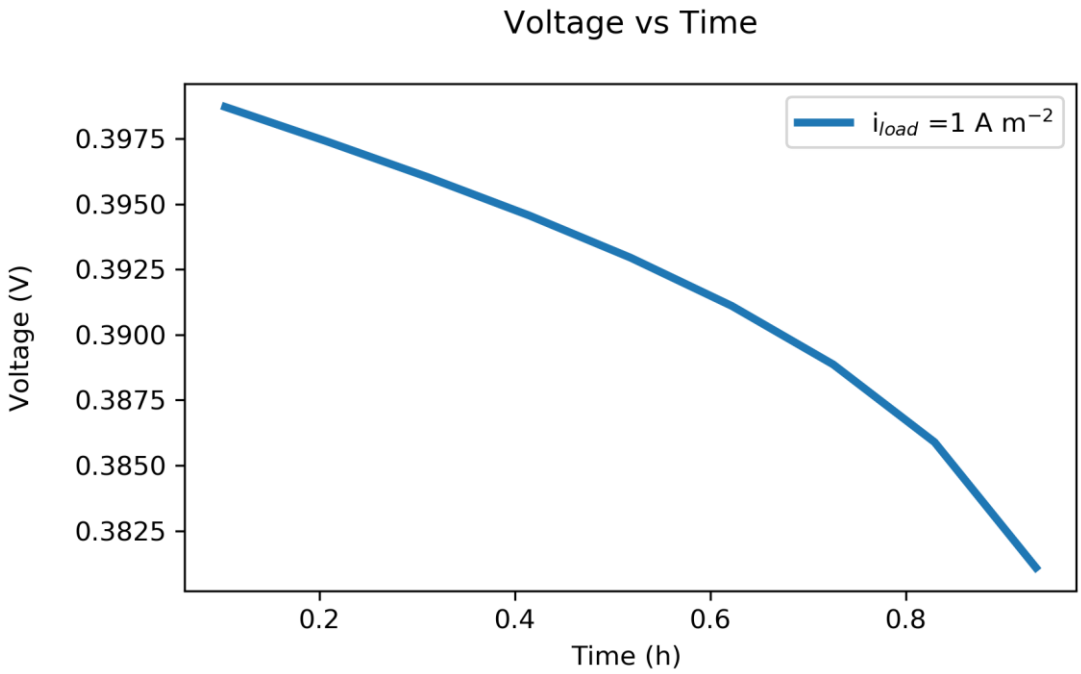

Figure 16. The cathode potential

7.3 The Precipitation of $Mg(OH)_2$

As a result of the anodic reaction, the magnesium started to dissolve into the electrolyte and formed $Mg(OH)_2$. This created a concentration gradient adjacent to the interface in the electrolyte. Thus, the $Mg(OH)_2$ started to spread in the electrolyte in a manner described by the equation 25. The reaction proceeded until the amount of concentration, across the electrolyte, converged to approximately uniform value. The precipitation of $Mg(OH)_2$ into electrolyte is depicted in Figure 17.

On the graph, the curves represent the amount of concentration at different locations in the electrolyte. The yellow curve represents the location at a point just next to the magnesium anode. Therefore, it has the highest concentration at the beginning of the discharge and also the steepest drop in concentration during the reaction. The green curve on the other hand, represents the location at the farthest point from the anode which is the reason why it has the longest delay in the increase of concentration. The blue and red curves represent points closer to the centre of the electrolyte. Initially, the blue curve experienced a large rise in concentration as a large portion of $Mg(OH)_2$ precipitated towards the other end of the electrolyte. This caused the concentration of $Mg(OH)_2$ to rise even past the

converge point. Afterwards, the rise of concentration changed to a steady decline as the electrolyte slowly approached a uniform value of concentration. The red curve experienced similar fluctuation but not as high because it is located at a point farther away from the anode. As shown on the x-axis, the precipitation of $Mg(OH)_2$ is time-consuming process. This is due to the slow diffusivity of $Mg(OH)_2$ (7×10^{-10} m^2 s^{-1}) in aqueous solutions. Evidently, all curves converge to the same concentration of the electrolyte.

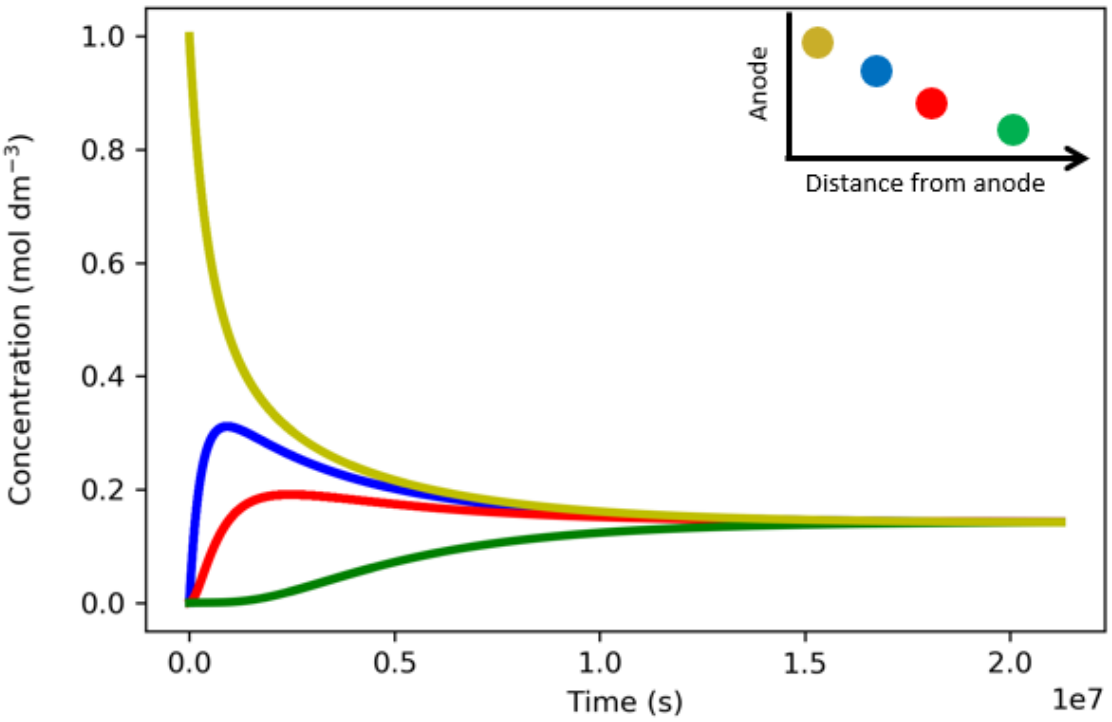

Figure 17. The precipitation of $Mg(OH)_2$.

Figure 18 illustrates a graphical representation of the precipitation reaction. The area in the graph represents the electrolyte. The left side of the electrolyte is the anode side. The colour bar next to the graph indicates the amount of concentration. In the last graph, the yellow curve represented a point located at the upper-left corner of the electrolyte. The green curve on the other hand, was located at a point at the lower-right corner. The red and blue curves were located in between the two. At initial stages of the precipitation reaction, the concentration of $Mg(OH)_2$ was highest at the interface. As the reaction proceeded, the $Mg(OH)_2$ started to slowly spread until the amount of concentration converged to approximately the same values across the electrolyte. This is illustrated with uniform colour.

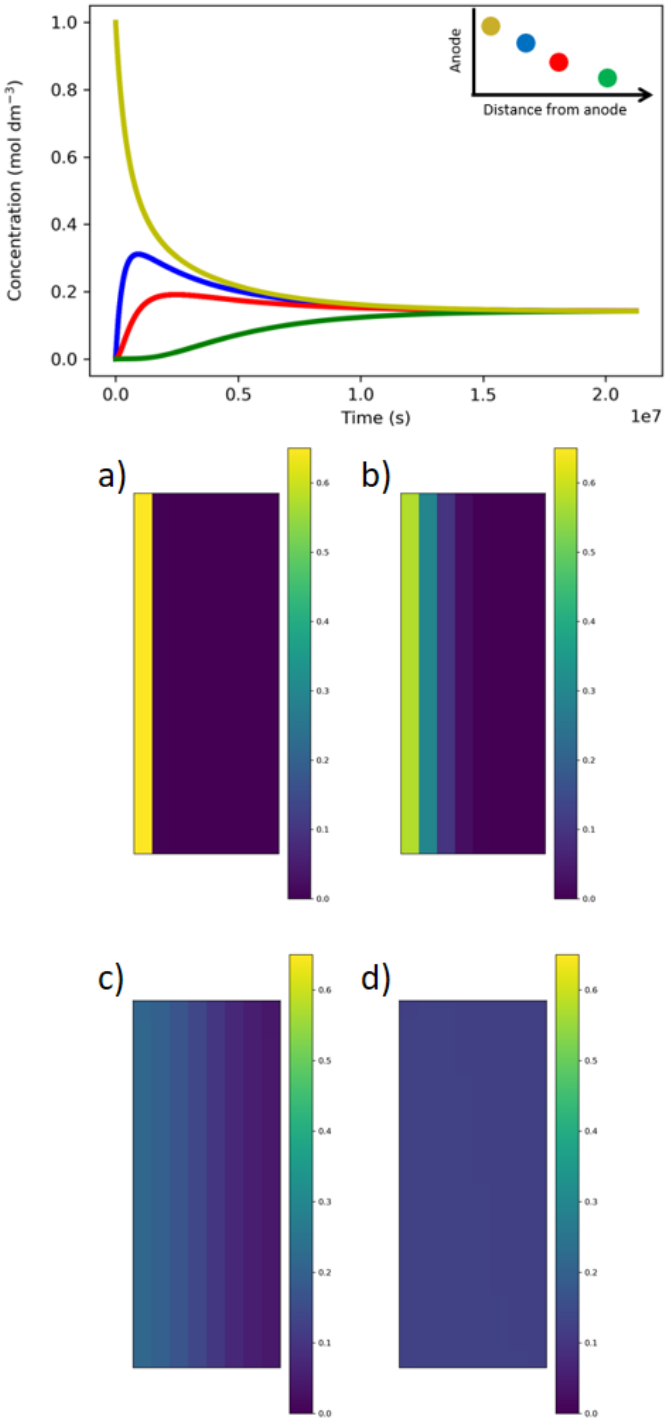

Figure 18. Change in concentration in the electrolyte at different points in time: a) at 0 seconds, b) after 1.0×10^5 seconds, c) after 4.8×10^6 seconds, d) after 2×10^7 seconds.

7.4 The Cell

7.4.1 The Cell Potential and Current

Figure 19 depicts the potential curve of the entire magnesium-air cell. It consists of both anode and cathode potentials, described by the Nernst equation. The cell voltage drops as a consequence of combined overpotentials from both electrodes. Identical to the electrode reactions, the rate of the cell potential drop, due to structural alternations, is steady at the initial stages of the discharge. As the discharge process approached a point where nearly all magnesium in the anode had been exhausted, there was a sharp increase in rate of potential drop. The cell reaches the end of discharge voltage around 3.03 V (vs. SHE) when the whole anode has been depleted of magnesium.

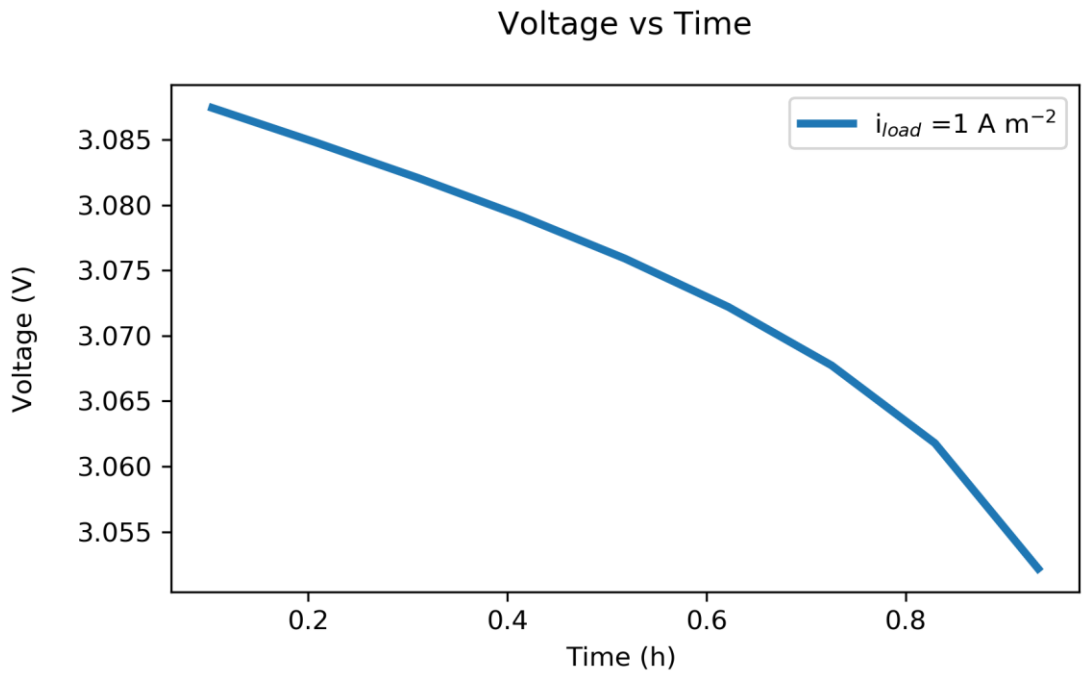

Figure 19. Cell Potential

The cell current density is shown in Figure 20. As described by the Butler-Volmer equation, it is obtained as a difference between anodic and cathodic current densities. As seen on the graph, the cell current density increased with the same rate as the cell potential decreased.

This can be explained with equations 17 and 21. In order for the overpotential to increase, there has to be a decrease in the cell potential, as described by the equation 17. At the same time, the increase in overpotential led to an increase in the cell current density, as stated in the Butler-Volmer equation.

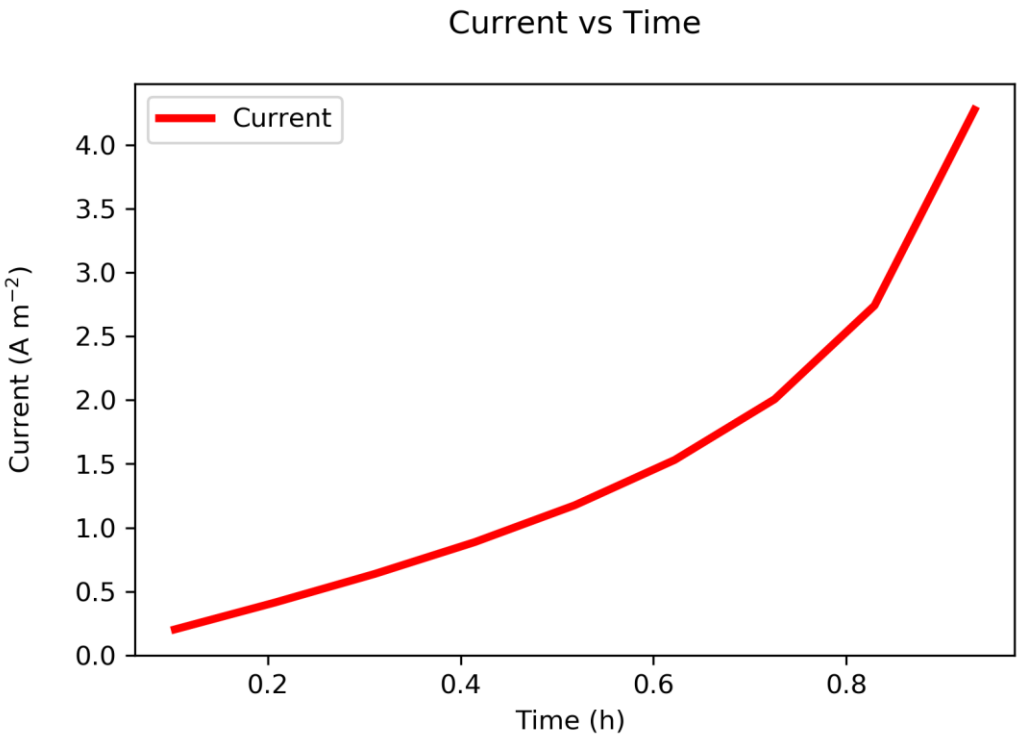

Figure 20. The cell current density.

7.4.2 The Cell Capacity

Figure 21 depicts capacity versus cell voltage. The curves represent the cell potential under different load. The results show that a heavy load leads to a significant drop in the cell potential which shows as a lower capacity of the cell.

This can be explained with mass balance. As it has been previously stated, the flux of species is diffusion-limited in the electrolyte. During the heavier loads, there is a higher demand for electron-transfer with a faster rate of reaction than the particles in the cell can provide. Consequently, only a portion of active material in anode took part in the electron-transfer reaction. This results in rapidly dropping potential and limited cell capacity as some of the active material remain inactive during the discharge. /22, 41/

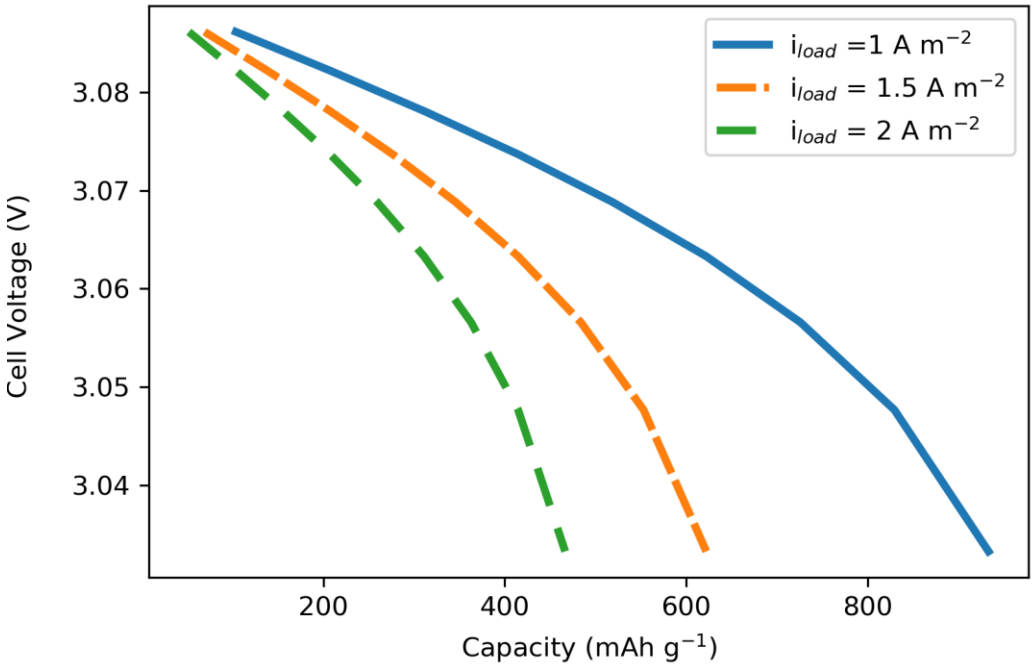

Figure 21. Cell capacity under different load current densities.

7.5 Comparison to Experimental Data

Figure 22 compares the simulation results to experimental data. The experimental data depicts a voltage-capacity curve of Mg-Al-Mn alloy (AM60) anode /52/. Despite being a two-dimensional model, the behavior of the simulated cell shows a trend similar to the experimental unit. The experiment was carried out with a load current of 2.5 mA/cm^2 (25 A m^{-2}) while the curve in the simulation result was produced by a load current of 1 A/m^2. The shapes of the potential curves in Figure 22 resemble each other. However, the resulting values vary due to a number of reasons.

First, in the simulation, the rate of reaction was assumed due to lack of directly applicable data. This affects the potential-capacity curve as the duration of the reaction is an essential part of the capacity equation (equation 22). Furthermore, the experimental anode had different chemical composition than the simulated one. Mg-Al-Mn alloy was used as anode material in the experiment, while the simulated cell used pure magnesium metal. Moreover, in the experiment, the anode was a physical electrode while the simulation used two-dimensional representation of the Mg anode. Finally, the experimental results include multistep reaction mechanism and parasitic reactions, such as corrosion and formation of

passivating film, while the simulation cell was simplified to one-step reaction mechanism without any parasitic reactions. These factors affect the shape of the curve and operating voltage of the results. /52/

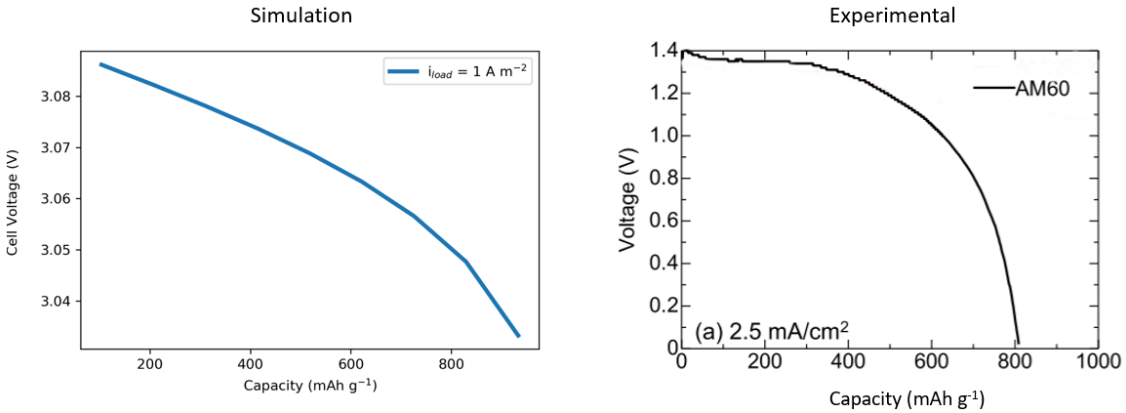

Figure 22. Comparison of simulation and experimental results obtained from /52/.

8 CONCLUSION

In this thesis, a two-dimensional mathematical model was developed for magnesium-air battery. The governing equations were deduced from mass balance and electrochemical kinetics. Numerical methods were used to solve the governing equations. Based on these solutions, a computational simulation was developed in the Python programming language. The simulation was used to predict the electrochemical performance of the cell. Recognizing the accuracy of the model could be improved, it still represented theoretical performance of the cell.

In the simulation, the discharge of the cell was carried out under predetermined conditions. The rate of change of Mg to $Mg(OH)_2$ was determined and graphically represented using OVITO. The precipitation of $Mg(OH)_2$ in the electrolyte was also analysed and graphically displayed. During the discharge, the concentration of $Mg(OH)_2$ was shown to converge to approximately uniform value in the electrolyte.

The cell potential and current density results were obtained from the simulation. The numerical results showed that at the initial stages of discharge, the cell potential declined steadily due to increasing overpotential. Afterwards, the cell experienced a sharp drop in potential as the available active material approached depletion. On the other hand, the cell current density curve was shown to follow the rise of the overpotential. Furthermore, the impacts of various load current densities on the discharge capacity were predicted. The results indicate that the magnitude of a load current has a noticeable impact on the cell capacity. Moreover, the results of the model were compared to previous experiments. Despite the limitations of the simplified two-dimensional model, the model output matches the experimental data in behaviour.

In the future, the model could be used to optimize magnesium-air battery performance. To improve the accuracy of the results, the mathematical model could be further developed by including parasitic reactions, such as corrosion and hydrogen evolution reaction. It could also be modified into a three-dimensional model, making the results closer to reality.

REFERENCES

/1/ Luo, X., Wang, J., Dooner, M. & Clarke, J. 2015. Overview of current development in electrical energy storage technologies and the application potential in power system operation. Applied Energy. Elsevier. 137, 511–536.

/2/ Holden, E., Linnerud, K. & Banister, D.2014. Sustainable development: Our Common Future revisited. Global Environmental Change. Elsevier. 26, 130–139.

/3/ Anvari, M., Lohmann, G., Wächter, M. Milan, P., Lorenz, E., Heinemann,D:, Tabar, M. R. R. & Peinke J. 2016. Short term fluctuations of wind and solar power systems. New Journal of Physics. IOP publishing. 18.

/4/ Robison, A.P., Blyther, P.T., Bell, M.C., Hübner, Y. & Hill, G.A. 2013. Analysis of electric vehicle driver recharging demand profiles and subsequent impacts on the carbon content of electric vehicle trips. Energy Policy. Elsevier. 61, 337–348.

/5/ Chandra Mouli, G.R., Bauer, P. & Zeman, M. 2016. System design for a solar powered electric vehicle charging station for workplaces. Applied Energy. Elsevier. 168, 434–443.

/6/ Lee, J-S., Kim, S. T., Cao, R., Choi, N-S., Liu, M., Lee, K. T. & Cho, J. 2011. Metal-Air Batteries with High Energy Density: Li-Air versus Zn-Air. Weinheim. WILEY-VCH Verlag GmbH & Co. 1, 1, 34–50.

/7/ Li, Y. & Dai, H. 2014. Recent advance in zinc-air batteries. Chemical Society Reviews. 43, 15, 5257–5275.

/8/ Thangavel, V., Xue, X-H., Mammeri, Y., Quiroga, M., Mastouri, A., Quéry, C., Johansson, P., Morcrette, M. & Franco, A. A. 2016. A Microstructurally Resolved Model for Li-S Batteries Assessing the Impact of the Cathode Design on the Discharge Performance. Journal of The Electrochemical Society. ECS. 163, 3, 2817–2829.

/9/ Cheng, F. & Chen, J. 2012. Metal-air batteries: from oxygen reduction electrochemistry to cathode catalysts. Chemical Society Reviews. RSC Publishing. 58, 538–588.

/10/ Rahman, Md. A., Wang, X. & Wen, C. 2013. High Energy Density Metal-Air Batteries: A review. Hawthorn. The Electrochemical Society. 160, 10, 1759–1771.

/11/ Zhang, T., Tao, Z. & Chen, J. 2014. Magnesium-air batteries: from principle to application. Royal Society of Chemistry. 2, 196–206.

/12/ Mokhtar, M., Talib, M. Z. M., Majlan, E. H., Tasirin, S. M., Ramli, W. M. F. W., Daud, W. R. W. & Sahari, J. 2015. Recent developments in materials for aluminium-air batteries: A review. Journal of Industrial and Engineering Chemistry. Elsevier B.V. 32, 1–20.

/13/ Shu, C., Wang, E., Jiang, L. & Sun, G. 2013. High performance cathode based on carbon fiber felt for magnesium-air fuel cells. International Journal of Hydrogen Energy. Elsevier. 38, 14, 5885–5893.

/14/ Tsutsumi, A. 2013. Fuel cell/battery system. Tansei. Institute of Industrial Science. 10.

/15/ Liu, Y., Sun, Q., Li, W., Adair, K. R., Li, J. & Sin, X. 2017. A comprehensive review on recent progress in aluminum-air batteries. Green Energy & Environment. Kea Ai publishing. 2, 3, 246–277.

/16/ Wang, J. 2000. Analytical electrochemistry. Second edition. New York. A John Wiley & Sons.

/17/ Bard, A. & Faulkner, L. 2000. Electrochemical methods. Fundamentals and Application. Second Edition. Phoenix. A John Wiley & Sons.

/18/ Zhang, X., Wang, X-G., Xie, Z. & Z, Z. 2016. Recent progress in rechargeable alkali metal-air batteries. Green Energy & Environment. Ke Ai publishing. 1, 1, 4–17.

/19/ Kiehne, H. A. 2003. Battery Technology Handbook, Second Edition. USA. Expert Velag.

/20/ Wang, N., Wang, R., Peng, C. & Feng, Y. 2014. Enhancement of the discharge performance of AP65 magnesium alloy anodes by hot extrusion. Corrosion Science. Elsevier. 81, 85–95.

/21/ Xiong, H., Yu, K., Yin, X., Dai, Y., Yan, Y. & Zhu, H. 2017. Effects of microstructure on the electrochemical discharge behavior of Mg-6wt%Al-1wt%Sn alloy as anode for Mg-air Primary battery. Journal of Alloys and Compounds. Elsevier. 708, 652–661.

/22/ Kim. S. U., Perdue, B., Apblett, C. A. & Srinivasan, V. 2016. Understanding Performance Limitations to Enable High Performance Magnesium-Ion Batteries. Journal of The Electrochemical Society. ECS. 163, 8, 1535–1542.

/23/ Rumble, J. R. 2018. CRC Handbook of Chemistry and Physics. 98th Edition (Internet Version). Boca Raton, FL. CRC Press/Taylor & Francis.

/24/ Zhang, T., Imanishi, N., Shimonishi, Y., Hirano, A., Xie, J., Takeda, Y., Yamamoto, O. & Sammes, N. 2010. Stability of a Water-Stable Lithium Metal Anode for a Lithium-Air Battery with Acetic Acid-Water Solutions. Journal of The Electrochemical Society. ECS. 157, 2, 214–218.

/25/ Mao, Z. & White, R. E. 1992. Mathematical Modelling of a Primary Zinc/Air Battery. Journal of the Electrochemical Society. ECS. 139, 4, 1105–1113.

/26/ Zhang, H. & Ruitao, L. 2018. Defect engineering of two-dimensional materials for efficient electrocatalysis. Journal of Materiomics. The Chinese Ceramic Society.

/27/ Grande, L., Paillard, E., Hassoun, J., Park, J.-B., Lee, Y.-J., Sun, Y.-K., Passerini, S. & Scrosati, B. 2014. The Lithium/Air Battery: Still an Emerging System or a Practical Reality. Advanced Materials. Germany. WILEY-VCH Verlag GmbH & Co. 27, 5, 748–800

/28/ Chen, L. D., Nørskov, J. K. & Luntz, A. C. 2015. Theoretical Limits to the Anode Potential in Aqueous Mg-Air Batteries. The Journal of Physical Chemistry. American Chemical Society. 119, 34, 19660–19667.

/29/ Khoo, T., Howlett, P. C., Tsagouria, M., MacFarlane, D. R. & Forsyth, M. 2011. The potential for ionic liquid electrolytes to stabilize the magnesium interface for magnesium/air batteries. Electrochimica Acta. Elsevier. 43, 15, 5257–5275.

/30/ Li, C-S., Sun, Y., Gebert, F. & Chou, S-L. 2017. Current Progress on Rechargeable Magnesium-Air Battery. Progress Report. Advanced Energy Materials. WILEY-VCH Verlag GmbH & Co. 7, 24, 1700869

/31/ Smith, J. G., Naruse, J., Hiramatsu, H. & Siegel, D. J. 2016. Theoretical Limiting Potentials in Mg/O_2 Batteries. Chemistry Materials. American Chemical Society. 28, 5, 1390–1401.

/32/ Hasvold, Ø., Henriksen, H., Melvær, E., Citi, G., Johansen, B. Ø., Kjønigsen, T. & Galetti, R. 1997. Sea-water battery for subsea control system. Journal of Power Sources. Elsevier. 65, 1–2, 253–261.

/33/ Richey, F. W., McCloskey, B. D. & Luntz, A. C. 2016. Mg Anode Corrosion in Aqueous Electrolytes and Implications for Mg-Air Batteries. Journal of The Electrochemical Society. ECS. 163, 6, 958–963.

/34/ Esmaily. M, Svensson, J. E., Fajardo, S., Birbilis, N., Frankel, G. S., Virtanen, S., Arrabal, R., Thomas, S. & Johansson, L. G. 2017. Fundamentals and advances in magnesium alloy corrosion. Progress in Materials Science. Elsevier. 89, 92–193.

/35/ Shao, H., Ma., W., Kohno. M., Takata, Y., Xin, G., Fujikawa, S., Fujino, S., Bishop, S. & Li, X. 2014. Hydrogen storage and thermal conductivity properties of Mg-based materials with different structures. International Journal of Hydrogen Energy. Elsevier. 39, 18, 9893–9898.

/36/ Reggiani, P., Sivapalan, M. & Hassanizadeh, M. S. 2000. Conservation equations governing hillslope responses: Exploring the physical basis of water balance. Water Resources Research. American Geophysical Union. 36, 7, 1845–1863.

/37/ Soderberg, J. N., Co, A. C., Sirk, A. H. C. & Birss, V. I. 2006. Impact of Porous Electrode Properties on the Electrochemical Transfer Coefficient. The Journal of Physical Chemistry. American Chemical Society. 110, 21, 10401–10410.

/38/ Zhao, X. & Huang, K. 2013. Solid Oxide Iron-Air Rechargeable Battery – A new Energy Storage Mechanism. ECS Transaction. The Electrochemical Society. 50, 45, 115–123.

/39/ Sandhu, S. S., Fellner, J. P. & Brutchen, G. W. 2007. Diffusion-limited model for a lithium/air battery with an organic electrolyte. Journal of Power Sources. Elsevier. 164, 1, 365–371.

/40/ Deiss, E., Holzer, F. & Haas, O. 2002. Modeling of an electrically rechargeable alkaline Zn-air battery. Electrochimica Acta. Elsevier. 47, 25, 3995–4010.

/41/ Clark, S., Latz, A. & Horstmann, B. 2018. A Review of Model-Based Design Tools for Metal-Air Batteries. Batteries. MDPI. 4, 5.

/42/ Noren, D. A. & Hoffman, M. A. 2005. Clarifying the Butler-Volmer equation and related approximations for calculating activation losses in solid oxide fuel cell models. Journal of Power Sources. Elsevier. 152, 175–181.

/43/ Torayev, A., Rucci, J., Magusin, P. C. M. M., Demortiere, A., Andrade, V. D., Grey, C. P., Merlet, C. & Franco, A. A. 2018. Stochasticity of Pores Interconnectivity in Li-O Batteries and its Impact on the Variations in Electrochemical Performance. The Journal of Physical Chemistry Letters. ACS Publications. 9, 4, 791–797.

/44/ Yoo, K., Banerjee, S. & Dutta, P. 2014. Modeling of volume change phenomena in a Li-air battery. Journal of Power Sources. Elsevier. 258, 340–350.

/45/ Menzies, N. 2009. The Science of Phosphorus Nutrition: Forms in the Soil, Plant Uptake, and Plant Response. GRDC Update Papers. GRDC Grains Research & Development Corporation.

/46/ Blanquer, G., Yin, Y., Quiroga, M. A. & Franco, A. A. 2016. Modeling Investigation of the Local Electrochemistry in Lithium-O_2 Batteries: A Kinetic Monte Carlo Approach. Journal of The Electrochemical Society. ECS. 163, 3, 329–337.

/47/ Chapra, S. & Canale, R. 2015. Numerical Methods for Engineers, Seventh Edition. McHraw-Hill Education.

/48/ Seshu, P. 2012. Textbook of Finite Element Analysis. PHI.

/49/ Downey, A. 2012. Think Python: How to Think Like a Computer Scientist. Needham MA. Green Tea Press.

/50/ Raybaut, P. 2017. Spyder documentation, Release 3.

/51/ Stukowski, A. 2010. Visualization and analysis of atomistic simulation data with OVITO- the Open Visualization Tool. Modelling and Simulation in Materials Science and Engineering. 18, 1.

/52/ Yuasa, M., Huang, X., Suzuki, K., Mabuchi, M. & Chino, Y. 2015. Discharge properties of Mg-Al-Mn-Ca and Mg-Al-Mn alloys as anode materials for primary magnesium-air batteries. Journal of Power Sources. Elsevier. 297, 449–456.